ESTABLISHING A CISPLATIN-RESISTANT TRIPLE NEGATIVE BREAST CANCER SPHEROID MODEL

Ongeziwe Ngalonkulu

Student number: 2021926635

Submitted in partial fulfilment of the requirements in respect of the master's degree MMedSci Pharmacology in the Department of Pharmacology in the Faculty of Health Sciences at the University of the Free State

31 JULY 2024

SUPERVISOR	CO-SUPERVISOR	CO-SUPERVISOR
Prof Mamello Sekhoacha, Department of Pharmacology University of the Free State	Dr Beynon Abrahams, Department of Basic Medical Sciences University of the Free State	Prof Chrisna Gouws, Pharmacen™ North-West University

Declaration of authorship

I, Ongeziwe Ngalonkulu, declare the following:

The dissertation that I herewith submit for the master's degree in medical sciences (Pharmacology) at the University of the Free State is my independent work, and that I have not previously submitted it for a qualification at another institution of higher education."

The research reported in this dissertation (including the research protocol), except where otherwise indicated, is my original work. This dissertation does not contain other persons' data or writing unless specifically acknowledged as being sourced from other researchers, attributed to them and referenced appropriately.

No part of the dissertation was generated by artificial intelligence. The entire content, including the protocol, research, analysis and writing, results from human effort, intellect, and original thought.

Supervisor Declaration

UNIVERSITY OF THE FREE STATE
UNIVERSITEIT VAN DIE VRYSTAAT
YUNIVESITHI YA FREISTATA
UFS HEALTH SCIENCES

26 July 2024

Regarding Ongeziwe Ngalonkulu's submission of master's dissertation for examination:

Supervisor's declaration

I, **Professor Mamello Sekhoacha**, the supervisor of the master's research dissertation entitled: **Establishing a cisplatin-resistant triple negative breast cancer spheroid model**, hereby certify that the work in this project was done by **Ongeziwe Ngalonkulu (student no. 2021926635)** at the Department of Pharmacology, University of the Free State. I hereby approve the submission of this thesis and also affirm that this has not been submitted previously, either in part or in its entirety, to the assessors, neither to this or any other institution for admission to a degree or any other qualification.

Date .....26 July 2024..... Signature ....

205 Nelson Mandela Drive | Park West, Bloemfontein 9301 | South Africa
P.O. Box 339 | Bloemfontein 9300 | South Africa | www.ufs.ac.za

VISION 130 Renew and Reimagine for 2034

Dedication

I proudly dedicate this thesis to myself, Ongeziwe Ngalonkulu, for my unwavering determination and resilience. Through it all, I have remained committed to my academic pursuits, and this is a testament to my hard work.

Acknowledgments

Supervisor and co-supervisors: Professor Mamello Sekhoacha, for her unwavering guidance, expertise, and support throughout this journey. Her patience, encouragement, and insightful feedback have been invaluable to me.

Professor Chrisna Gouws, for her contributions to this research project, academic growth, and opportunities. Her expertise and input have significantly enhanced the quality of this work.

Dr Beynon Abrahams, for his assistance and mentorship. His guidance and support have helped shape my research and helped me navigate this journey.

My Laboratory Partner, Viwe Fokazi, for her dedication to our shared goals; together, we navigated challenges, celebrated successes, and grew as researchers. I appreciate the memories we have shared and am honored to have had the opportunity to work alongside her.

My Family: I would like to express my deepest gratitude to my family for believing in me, their encouragement, and help in my time of need. Your love and support meant the world to me, and I dedicate this achievement to all of you.

Most importantly, I thank God, the source of all wisdom and knowledge, for granting me the physical and mental health to undertake and complete this research.

I would also like to acknowledge the University of the Free State, the Faculty of Health Sciences, Department of Pharmacology and Basic Medical Sciences, as well as the North West University, Centre of Excellence for Pharmaceutical Sciences (Pharmacen™) for the evaluation of this project and valuable suggestions during the execution of this project—the National Research Foundation (NRF) for financial support for completing this degree.

Table of Contents

Abstract

In cancer research, conventional two-dimensional (2D) cell cultures and animal studies are often used in studying the disease and efficacy of anticancer agents despite their failure to accurately replicate the complex *in vivo* tumour microenvironment. 2D cultures lack the extracellular matrix production critical for *in vivo*-like cell behaviour, thereby jeopardizing data accuracy when developing effective cancer therapies and understanding mechanisms underlying drug resistance and cancer relapse. There is, therefore, a pressing need for models that accurately recapitulate *in vivo* systems and enhance researchers' accuracy in predicting disease mechanisms. This study aimed to establish a cisplatin-resistant three-dimensional (3D) spheroid model using the scaffold-free technique of rotating wall bioreactors in the CelVivo ClinoStar™ system, to facilitate efficient recapitulation of *in vivo*-like conditions and higher throughput.

The MDA-MB-231 cell line is classified as triple negative breast cancer (TNBC) due to the absence of the oestrogen receptor and progesterone receptor, as well as the human epidermal growth factor receptor 2. As a result, the MDA-MB-231 cell line is characterized as a highly metastatic and aggressive cell line with a poor prognosis. Cisplatin-resistant MDA-MB-231 cells were generated by exposing the cell line to IC_{10}-IC_{50} (0.01µM, 0.1µM, 1µM, 5µM and 10µM) concentrations of cisplatin for nine months. The cells acquired resistance; these resistant cells were then used to develop a 3D spheroid model. Characterization of the cisplatin-resistant MDA-MB-231 spheroids over 28 days included assessing spheroid growth and viability, and identifying the optimal experimental window between days 12 and 22. The model's reactivity to cisplatin and doxorubicin treatment was evaluated for 96 hour (h) to qualify the model for treatment screening. Treatment with the clinical cisplatin dose (4,435 x 10^{-6} µg cisplatin/µg protein) showed pronounced reactivity after 48 h, with decreased cell viability and increased cell death. However, spheroids recovered after 72-96 h, displaying moderate to high metabolic activity, typical of resistance. The IC_{50} (8.06 x 10^{-2} µg cisplatin/µg protein) dose of cisplatin demonstrated immediate effects on the model after 48 h, however, increase in spheroid size and decrease in cell death was observed with increased metabolic activity after apparent recovery at 72-96 h suggesting resistance. Treatment

with doxorubicin clinical dose (1.064 x 10^{-5}µg dox/µg protein) had the most pronounced effect on the model throughout the 96 h and resulted in decreased spheroid size. It was apparent that the model was not as resistant to the doxorubicin treatment as it was to the cisplatin treatment. This model has potential for preclinical research studies as it displays reactivity to commonly used chemotherapeutic drugs and could be valuable in understanding drug-resistant cancer. In conclusion, the established cisplatin-resistant MDA-MB-231 3D spheroid model offers a robust platform for studying drug effects in TNBC research.

Keywords: CelVivo ClinoStar™, cisplatin resistance, spheroid model, three-dimensional cell culture, triple negative breast cancer, two-dimensional cell culture.

List of Abbreviations

Abbreviation	Definition
ABC	ATP-binding cassette
ADM	Adriamycin
AK	Adenylate kinase
ANOVA	Analysis of Variance
ATCC	American Tissue Culture Collection
ATP	Adenosine triphosphate
BCSCs	Breast cancer stem cells
BMI	Body mass index
BSA	Bovine serum albumin
CSCs	Cancer stem cells
DMEM	Dulbecco's modified eagle medium
DMSO	Dimethyl sulfoxide
DNA	Deoxyribonucleic acid
DOX	Doxorubicin
DTX	Docetaxel
EBREC	Environmental and Biosafety Research Ethics Committee

ECM	Extracellular matrix
EMT	Epithelial-Mesenchymal Transition
EMT-TFs	Epithelial-to-mesenchymal transition transcription factors
EPI	Epirubicin
FBS	Foetal Bovine serum
GFs	Growth factors
GLOBOCAN	Global Cancer Statistics 2020
HDI	Human Development Index
MDR	Multidrug resistance
MIN	Minutes
MIR	Mortality-to-incidence ratio
MTT	3-(4,5-dimethylthiazol-2-yl)-2,5-diphenyltetrazolium bromide
OSHA	Occupational Safety and Health Administration
PBS	Phosphate-buffered saline
PR	Progesterone receptor
PROF	Professor
REC	Research Ethics Committee
TNBC	Triple-negative breast cancer
WHO	World Health Organisation

List of Figures

CHAPTER 1- INTRODUCTION

Cancer is a complex disease denoted by alterations in the cell physiology that result in malignant tumours. The primary cause of illness and mortality in most cancer patients is tumour cell invasion of neighbouring tissues and organs (Seyfried and Huysentruyt, 2013). Breast cancer is the most common type of cancer malignancy in women and the leading cause of mortality in this group (Nardin et al., 2020). According to Global Cancer Statistics (GLOBOCAN, 2020), breast cancer has been diagnosed as the most malignant beyond lung cancer, with 2.3 million cases yearly (11.7%), followed by lung cancer at 11.4%, colorectal cancer at 10.0%, prostate cancer at 7.3%, and lastly, stomach cancer 5.6% (Sung et al., 2021).

Triple-negative breast cancer (TNBC) is one of the most aggressive and highly metastatic types of breast cancer, resistant to hormonal and human epidermal growth factor receptor 2 (HER2)-targeted antibody therapy (Kassam et al., 2009). This disease is reported to be more frequent in older women as well as women of the African and Hispanic backgrounds (Derakhshan and Reis-Filho, 2022). TNBC is characterized by a short overall survival duration, owing primarily to the lack of specialized therapeutic methods. However, in advanced TNBC, chemotherapy is preferred because it is the most effective treatment option to treat and manage symptoms, as surgery is considered costly and highly invasive (DeSantis et al., 2019). Some of the chemotherapeutic drugs employed to eradicate breast cancer include anthracyclines such as doxorubicin and epirubicin, as well as platinum-based drugs such as cisplatin and carboplatin (Kassam et al., 2009, Boichuk et al., 2017). As a first-generation platinum-based drug, cisplatin has been used widely to treat patients with various cancers (Brown et al., 2019). Although cisplatin is not considered the golden standard treatment for TNBC, there is a growing interest in utilising it in cancer facilities due to its remarkable anticancer properties (Petrelli et al., 2016). Ongoing clinical trials are investigating the efficacy of cisplatin as a potential

treatment for TNBC, examining its effectiveness both as a monotherapy and in combination with other therapeutic regimens (Hill et al., 2019b)

Nonetheless, in clinical observation, breast cancer patients still experience poor drug responses and tumour recurrences even after undergoing chemotherapy treatment (Harbeck and Gnant, 2017). Approximately 90% of failed chemotherapy is reported to be during the invasion and metastatic stages of cancers, usually related to acquired drug resistance, as a result of long-term use of chemotherapy (Wang et al., 2019). The two most common mechanisms in which cancer cells become resistant are intrinsic drug resistance, meaning they are drug-resistant before treatment, and acquired resistance, meaning cells develop resistance following exposure (Abad et al., 2020). Chemoresistance has necessitated more research to study drug efficacy and response in tumour cells (Eiro et al., 2019). Therefore, accurate models that closely resemble the tumour environment are needed to ensure quality of preclinical research results.

To date, two-dimensional (2D) *in vitro* cell culture models have been the most widely used method for studying cellular processes relating to cancer initiation and development and testing potential anticancer agents (Sant and Johnston, 2017). The 2D model however, does not accurately mimic the *in vivo* tumour microenvironment (TME) (Hoarau-Véchot et al., 2018). *In vivo* xenograft models, on the other hand, have a stromal component that is not derived from humans; thus, their growth rate is faster than that of primary human tumours, with a doubling time of months, and generally respond better to anticancer drugs (Cassidy et al., 2016). Oncology clinical trials using experimental models have now confirmed the importance of demonstrating the architecture of *in vivo* tumours with regards to the epithelial-stromal interface, vasculature, necrotic zones and invasive fronts, the exact pathophysiology of a tumour, and its cell-extracellular matrix (ECM) component (Drost and Clevers, 2018, Wong et al., 2019).

In vitro cell culture models in three dimensions (3D) have shown promising distinct advantages compared to 2D cell cultures by better replicating human physiology and phenotypic characteristics. Many 3D *in vitro* methods, such as spheroids and organoids, 3D bioprinting, and organs-on-chips, can validate drugs (van Rijt et al., 2023). However,

many of these models require additional validation before being extensively utilized in preclinical testing (Andersen et al., 2015).

Spheroids are self-aggregated cells that develop to closely replicate drug diffusion and drug efficacy better, as seen in human cells, compared to 2D cell cultures (Gong et al., 2015). These structures can be utilized in various cell types with different functions (Tuveson and Clevers, 2019).

The limitations reviewed in 2D cell culture and animal studies, such as the lack of cell-cell and ECM-cell signalling pathways and drug diffusion, have encouraged researchers to progressively switch from 2D to 3D cell studies, which are more representative of *in vivo* physiological architecture and tumour microenvironment (Huh et al., 2010). Therefore, it is clear that a transition from conventional cell culture models to new 3D screening models is necessary to study the effects and reactivity of cancer cells to cisplatin and doxorubicin in a more resembling preclinical setting. This study aimed to develop a cisplatin-resistant MDA-MB-231 spheroid model using the CelVivo™ ClinoStar™ system as a 3D model for cancer research *in vitro*. The establishment of this model was be further characterized according to the spheroid growth, metabolic activity, cell death, and evaluated for potential use in merging the gap between traditional *in vitro* culture models currently employed and more *in vivo* resembling 3D cell culture models.

1.2 RESEARCH CONTEXT AND SIGNIFICANCE

1.2.1 Problem statement

Developing targeted therapies for TNBC has been a major challenge due to its heterogeneity and poor prognosis. Hence, it is crucial to investigate models to improve the overall understanding of this cancer subtype. 2D *in vitro* cultures, in which cells are grown in a monolayer, have been used for many years to assess the biological activity of molecules such as therapeutics for various diseases. However, these monolayers often require cell seeding on flat surfaces like culture flasks, which cannot replicate the actual intricacy and architectural framework structure observed in the human body. The structure imparted by the parts of TME and its 3D organisation may contribute to the aggressive tumour behaviour, characterized by low survival rates and increased tumour recurrence in cancer patients (Quail et al., 2016).

3D models, as opposed to conventional 2D models, have been shown to represent the TME more accurately, and provide physiologically relevant microenvironments promising for assessing drug disposition that influence drug safety and efficacy early in the drug development process. Hence, this study investigated whether a drug-resistant MDA-MB-231 cell line can be cultured into a 3D spheroid model using a ClinoStar™ system and further characterize its response to treatment with cisplatin and doxorubicin chemotherapeutic drugs as a resistant spheroid.

1.2.2 Study rationale

Researchers around the world have explored several 3D cell culture models. The scaffold-free technique is the most preferred as it allows cells to aggregate into spheroids without reinforcement and minimizes the time to reproduce spheroid models. This study employed the ClinoStar™-based rotating bioreactor approach to grow a 3D spheroid model. Bioreactors use a slow vessel rotation to simulate microgravity, which keeps cells suspended while allowing them to aggregate into spheroids (Trujillo-de Santiago et al., 2019). A bioreactor enables the development of spheroids within a regulated

environment, with operating conditions that allow for temperature adjustments, pH, shear stress, nutritional availability, and removal of toxins. This device constantly mixes the oxygen and nutrients within the medium to reduce the concentrated layer that is seen on the surface level of monolayers (Smit et al., 2020). One of the key advantages of rotating reactors is that efficient gas and nutrient exchange occurs inside the bioreactors (Wrzesinski and J Fey, 2015). In addition, a variety of benefits of this method include its simplicity, large-scale production of 3D cultures, and long-term culture of 3D spheroids (Barrila et al., 2010).

1.2.3 Research Question

What are the biochemical characteristics such as protein expression, cellular metabolism, signalling pathways of a cisplatin-resistant triple-negative breast cancer (MDA-MB-231) spheroid model, and how do they respond to chemotherapeutic drugs (doxorubicin and cisplatin) following exposure?

1.2.4 Aim

This study aimed to develop and characterize a novel 3D cisplatin-resistant MDA-MB-231 TNBC cell model using the CelVivo™ ClinoStar™ bioreactor system and to assess the spheroid model's reactivity to treatment with cisplatin and doxorubicin.

1.2.5 Objectives

- To culture MDA-MB-231 cells in a 2D monolayer and induce cisplatin resistance.
- Develop a 3D cisplatin resistant MDA-MB-231 spheroid model from the 2D cell culture, using a ClinoStar™ rotating bioreactor system.
- Characterize the viability and growth of the 3D-resistant MDA-MB-231 spheroid model in terms of planimetry, soluble protein content, glucose consumption,

extracellular adenylate kinase (AK) levels, and intracellular adenosine triphosphate (ATP) content.

- Qualify the model for treatment screening by assessing reactivity to anticancer drug treatment (cisplatin) and cross-reactivity with the anticancer drug doxorubicin.

CHAPTER 2 - LITERATURE REVIEW

The 2D cell culture model precedes the animal studies stage before advancing to the human clinical trials (Breslin and O'Driscoll, 2013). Hence, 3D *in vitro* cancer models are emerging as an innovative method to address the disparity between 2D *in vitro* cell cultures and animal models as they accurately mimic *in vivo* tumours (Tosca et al., 2023). Different 3D *in vitro* models are being developed, including spheroids and organoids that aim to closely mimic the human TME (Gunti et al., 2021). Therefore, this literature reviews the basic concept of breast cancer and the mechanisms by which these cancer cells acquire cisplatin resistance. Furthermore, this chapter elaborates on the promising opportunity of 3D *in vitro* cell culture methods in representing the human physiological environment.

2.1 Background on cancer

Cancer hallmarks are essential traits that cells develop as they become cancerous, a concept first outlined by Hanahan and Weinberg in 2011. Looking at cancer as an accumulation of certain hallmarks, research has aimed to understand the origin of cancer, identify targets for prevention, and develop strategies to counteract various hallmarks and treat cancer (Hanahan and Weinberg, 2011). Carcinogens are believed to act by altering normal cells, inducing the hallmarks, and transforming them into cancerous cells. This occurs through various mechanisms affecting the different levels of the physiological organization (Smith et al., 2020). Cancer hallmarks include:

(i) Self-sufficiency in growth signals; ability to sustain cell proliferation by activating pathways that support constant growth and division (Gutschner and Diederichs, 2012).

(ii) Insensitivity to anti-growth signals: cancer cells retain the ability to evade programmed cell death (Elmore, 2007) and alter their metabolism in order to survive (Navarro et al., 2022).

(iii) Evading apoptosis: cancer cells become resistant to apoptosis mediated by death receptors (Sharma et al., 2019). Furthermore, cancer cells may modify their signalling pathways or downregulate death receptors to stop the apoptotic cascades initiated downstream of these receptors (Gómez-Virgilio et al., 2022).

(iv) Tissue invasion metastasis: an essential property of malignant tumours is their ability to invade and metastasize (Hanahan and Weinberg, 2011). The initial step in the spread of cancer involves detaching cancer cells from the original tumour and infiltrating neighbouring tissues (Talmadge and Fidler, 2010).

(v) Limitless replicative potential: a defining characteristic of cancer cells is their ability to support replicative immortality, enabling them to outlive typical cellular lifespan constraints like senescence seen in non-cancerous cells. This capacity, which involves multiple critical pathways, is necessary for the tumours' continued growth and proliferation (Hanahan and Weinberg, 2011).

(vi) Sustained angiogenesis: an essential characteristic of cancer development, the ability of cancer cells to form new blood vessels (Kuczynski et al., 2019). This process ensures Tumours receive enough oxygen and nutrients and eliminates waste, encouraging survival and replication.

2.2 Breast cancer prevalence

Breast cancer is the most prevalent cancer and the primary cause of cancer-related deaths among women globally. Over 684,996 fatalities worldwide at an age-adjusted incidence of 13.6/100,000 were caused by breast cancer (Ferlay et al., 2021). Despite having the highest incidence rates in industrialized nations, Asia and Africa accounted for 63% of breast-cancer related deaths worldwide in 2020 (Ferlay et al., 2021). The majority of breast cancer patients live in high-income nations; however, in low and middle-income

nations, the prognosis is reported to be much worse (Ginsburg et al., 2017). The global 5-year survival rate measured by the breast cancer mortality-to-incidence ratio (MIR) in 2020 was estimated at 0.30 (Ferlay et al., 2021). Given the clinical severity of breast cancer, the 5-year survival rates for localized and regional cancer were higher, ranging at 75-90% in places with developed healthcare systems such as Hong Kong, Singapore, and Turkey.

In South Africa, breast cancer incidence has been reported (Dlamini et al., 2024) to have increased steadily over 20 years (2000-2020) among all patients. These results are reflected in the South African National Cancer Registry as well as the International Association of cancer Registries. Though these registries do not reflect the same numbers due to the different strategies used to collect data, the number of new breast cancer cases has accumulated over the last 20 years. TNBC is one of the breast cancer types that have been diagnosed at high rates in South Africa, reflecting the prevalence of this subtype seen in the African American population of the USA (Newman and Kaljee, 2017).

2.3 Breast cancer risk factors

Breast cancer risk factors can be categorized as non-modifiable and modifiable risk factors, including gender (Nindrea et al., 2017). Females are generally at greater risk of being diagnosed with breast cancer and the reasons for this primarily relate to the composition of breast tissue and the hormonal influences that are usually prevalent in females. Throughout a woman's lifespan, the glandular tissue is prone to changes influenced by hormones, such as prolactin and oxytocin post-breastfeeding which impact the tissue and increase cancer development (Łukasiewicz et al., 2021). Genetics also pose a risk factor for being diagnosed with breast cancer, whereby the breast cancer gene 1 and breast cancer gene 2 are likely to be involved in mutations that increase the chances of developing cancer cells (Shiovitz and Korde, 2015). Additionally, studies show that race and ethnicity play a role in the development of breast cancer and contribute to the differences in how often it occurs, the mortality, and chances of survival (Łukasiewicz

et al., 2021). In the US, white non-Hispanic women have historically had the highest rates of breast cancer (Hill et al., 2019a). However, it is noted that while black women experience lower rates of breast cancer, they are more susceptible to higher mortality rates from breast cancer (ACS, 2014).

Research has identified modifiable risk factors for developing breast cancer, and some of these include obesity, which has been reported as one of the factors that increase the risk of postmenopausal breast cancer significantly (Mohanty and Mohanty, 2021). The adipose tissue produces the hormone oestrogen, and increased oestrogen levels stimulate the growth of hormone-sensitive breast cancer cells (Bhardwaj et al., 2019). Furthermore, researchers discovered that a higher body mass index (BMI) is linked to more aggressive biological characteristics of the tumour, such as a larger size and a higher percentage of metastasis. Breast cancer development has been linked to unhealthy diets that are high in saturated fats, which are generally found in animal products (Fiolet et al., 2018), and high consumption of alcohol. All these have been linked to obesity and being overweight, two conditions that are known to increase breast cancer risk (Leso et al., 2019). These substances disrupt hormonal balance and have oestrogenic properties; hence, exposure in adequate amounts has been reported to increase the chances of developing breast cancer-related mutations (Eve et al., 2020, Rodgers et al., 2018).

2.4 Triple-negative breast cancer

Clinically, breast cancer is classified based on immunohistochemical markers into four distinct types that are distinguished by their surface receptors: luminal A, luminal B, human epidermal growth factor receptor 2 (HER2)-positive, and triple-negative breast cancer (TNBC). TNBC, the most aggressive breast cancer, with absence of all surface receptors, oestrogen receptor (ER), progesterone receptor (PR), or HER2, and accounts for approximately 15-20% of all breast carcinomas. With an earlier age of initial onset, a greater likelihood of metastatic spread, and more frequent relapse, TNBC presents with a more aggressive clinical course than hormone receptor-positive or HER2-positive

cancers (Park et al., 2022, Garrido-Castro et al., 2019). The figure below illustrates in summary the most common breast cancer types with their respective receptors.

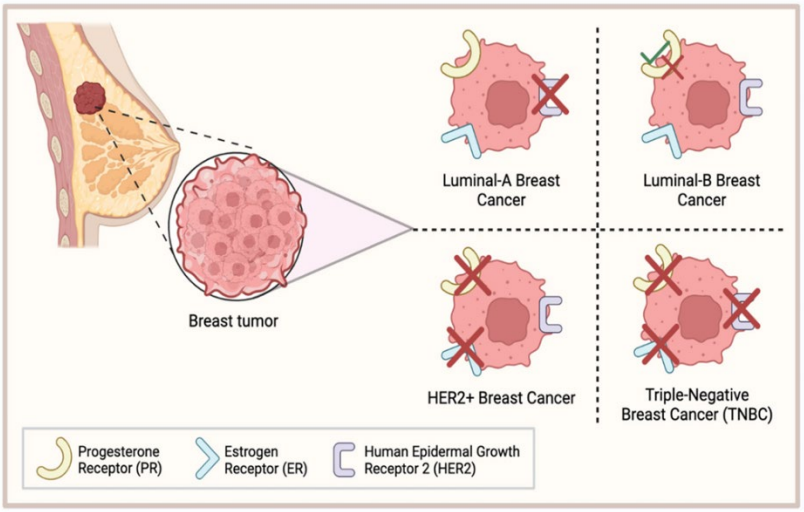

Figure 1. Classification of common breast cancers that show selective surface receptors (Kirkby et al., 2023).

2.4.1 Diagnosis of TNBC

Currently, TNBC is diagnosed using imaging and immunohistochemistry. Imaging comprises a mammogram, ultrasound of the breast, and magnetic resonance imaging (MRI) (Dass et al., 2021). A mammogram uses very low doses of radiation that cannot easily infiltrate the breast tissue to determine breast cancer through the presence of calcification or masses (Gosling et al., 2019). A challenge with mammography is the result of false negatives and positives, which can affect the patient's outcome (Hussaini, 2017). Additionally, the effects of radiation pose a significant risk for patients who are carriers of the breast cancer gene or have a family history of developing breast cancer (Wengert et al., 2019). Diagnosis of breast cancer using ultrasound is usually carried out when the mass or swelling is not located during mammography, however signs are observed (Dass et al., 2021). This method serves as an approach to differentiating between a breast cyst and a tumour. This differentiation is vital as it will assist in implementing the correct treatment method as breast cysts are often benign, whereas a tumour mass requires more testing to confirm malignancy (Berg et al., 2010).

The MRI diagnostic technique is utilized as an early detecting tool for individuals with a high risk of developing breast cancer due to its efficiency when compared to ultrasound and mammograms (Dogan et al., 2012). A limitation of using MRI is that it cannot distinguish the breast cancer subtype, and it only detects the presence of the cancer in the breast (Zhou et al., 2015).

The standard IHC technique is employed in pathological laboratories to diagnose TNBC, since the imaging techniques utilized in clinical facilities do not reveal the intratumoural characteristics such as necrosis and fibrosis commonly seen in TNBC (Penault-Llorca and Viale, 2012). This technique is based on detecting the ER, PR, and HER2 surface receptor markers (Oakman et al., 2010). These diagnostic techniques facilitate in developing the most effective outcomes for treating the disease and improve survival and quality of life.

2.4.2 Treatment of TNBC

The current treatment approach to breast carcinoma is multimodal, with the most common being surgery, radiotherapy, and chemotherapy.

2.3.2.1 Surgery

Most women diagnosed with breast cancer, report with early stages that can be treated with lumpectomy to remove a single lump with mastectomy, the removal of the breast tissue through surgical process (Kummerow et al., 2015). This procedure presents beneficial factors such as an improved survival rate, and patients can avoid radiation and chemotherapy altogether (Mamtani and Morrow, 2017). However, there are risks to this procedure; despite being highly invasive, it also presents with scarring, chronic pain, and anatomical changes of the chest area, affecting the shoulder girdle as well (Howes et al., 2017, Hidding et al., 2014). Additionally, the risk of breast asymmetry in a case of unilateral mastectomy has been reported as a major disadvantage to this treatment option (Hieken and Boughey, 2016).

2.3.2.2 Radiotherapy

Radiotherapy, on the other hand, is targeted at the whole breast and is based on the cancer type and size. This option is mostly a follow-up of the surgery procedure in case of recurrence (Gnant et al., 2017). The radiation risk include: incomplete treatment, resulting in rapid tumour growth recurrence, leading to poorer overall survival (Peart, 2015). Additionally, radiation can result in nerve damage and contractures (Lovelace et al., 2019).

2.3.2.3 Chemotherapy

TNBC are biologically aggressive and have been reported to be more responsive to chemotherapy than other breast cancer types, however, they still present with a poor prognosis (Wahba and El-Hadaad, 2015). The current therapeutic options for treating and managing TNBC include platinum compounds targeting the DNA repair pathway, anthracyclines targeting cell proliferation, and taxanes targeting P53 tumour suppressor (Wahba and El-Hadaad, 2015). These drugs work by killing rapidly growing cancer cells, however they are harmful to the healthy cells as they disrupt the cell cycle resulting in DNA damage and enforcing apoptosis (Alaouna et al., 2023). A significant limit of chemotherapeutic drug use is that they each present with toxicity and severe side effects such as fatigue, hair loss, and nausea/vomiting (Amjad et al., 2024). Anthracyclines such as doxorubicin, an antibiotic used for TNBC, present with a primary limit of permanently damaging the heart when given for prolonged durations and exceeding the administration dose (Rehman, 2018). Taxane use is reported to be halted by their side effect properties, which include gastrointestinal bleeding, with paclitaxel, the most commonly used for TNBC, being linked to cardiac conduction abnormalities (Ismail and Killeen, 2024).

2.3.2.3.1 Cisplatin

Cisplatin is a platinum compound with mild-to-moderate side effects compared to other chemotherapeutic agents, such as taxanes and anthracyclines used to treat TNBC. The side effects of the compound include myelosuppression, nephrotoxicity, neurotoxicity, and nausea/vomiting. Patients with metastatic breast cancer have reported high efficacy when using this chemotherapeutic drug in combination with other treatments (Baek et al., 2020). However, numerous research studies revealed that several patients with such

cancers eventually suffer from relapse and develop resistance to chemotherapy (Ranasinghe et al., 2022). Cancer cells become resistant to chemotherapeutic drugs through a variety of mechanisms, including changes in drug accumulation in cells through decreased uptake, detoxification of the drug, DNA repair, or negative regulation of apoptosis (Rabik et al., 2009, Galluzzi et al., 2012a, Zhu et al., 2018).

2.3.2.3.1.1 Mechanism of cisplatin resistance in cancer studies

During the treatment of solid tumours, cisplatin is administered intravenously as a short-term infusion dissolved in normal saline. Upon entering the cytoplasm, activation of cisplatin occurs through the displacement of chloride atoms by water molecules, which subsequently yields an electrophile that exhibits an affinity towards sulfhydryl groups present on proteins and nitrogen donor atoms on nucleic acids (Dasari et al., 2022). The binding selectivity of cisplatin to purine bases with 1, 2-intrastrand cross-links induces a disruption in cellular division and prompts apoptotic cell death (Brown et al., 2019).

It has been noted that resistance to cisplatin can develop in tumour cells upon failure to undergo apoptotic cell death after exposure to the drug at clinically relevant concentrations (Amable, 2016). Cisplatin resistance is a complex mechanism that cannot be explained by only a single molecular pathway; the processes leading to drug resistance are categorized based on the stage at which they transpire within the cell (Lugones et al., 2022).

The various ways that cisplatin resistance develops may include cisplatin being less effective at binding to the DNA because of accumulated detoxification processes or decreased drug concentrations within the cells (Galluzzi et al., 2012a). This may be due to increased glutathione synthesis and decreased levels of copper transporters, which prevent cisplatin from building up inside cells (Wangpaichitr et al., 2021). In the event that cisplatin does attach to DNA, cells can repair the damage by developing resistance to genetic harm or by using processes such as nucleotide excision repair (Galluzzi et al., 2014). Furthermore, despite DNA damage, modifications to signaling pathways, such as

the inactivation of TP53 and caspases, can stop cells from going through apoptosis or cell death. These resistance mechanisms have been found in ovarian and breast malignancies, among other types of cancer (Lugones et al., 2022).

Autophagy-mediated cisplatin resistance mechanism involves multiple cellular processes that protect cells against cisplatin-induced toxicity. Autphagy reduces cisplatin induced DNA damage by removing damaged mitochondria and other protein aggregates, thereby maintaining genomic stability (Kroemer et al., 2009). Addirionally, autophagy enhances DNA repair pathways, such as nucleotide excision repair, allowing cancer cells to repair DNA lesions more efficiently (Liu et al., 2013). Furthermore, autopahagy modulates apoptosis and necrosis, inhibiting pro-apoptotic signals and promotes cell survival (Galluzzi et al., 2012b).

A visual representation of these different pathways is shown in the image below, along with the corresponding molecules and enzymes in charge of each action that contributes to the compound's resistance.

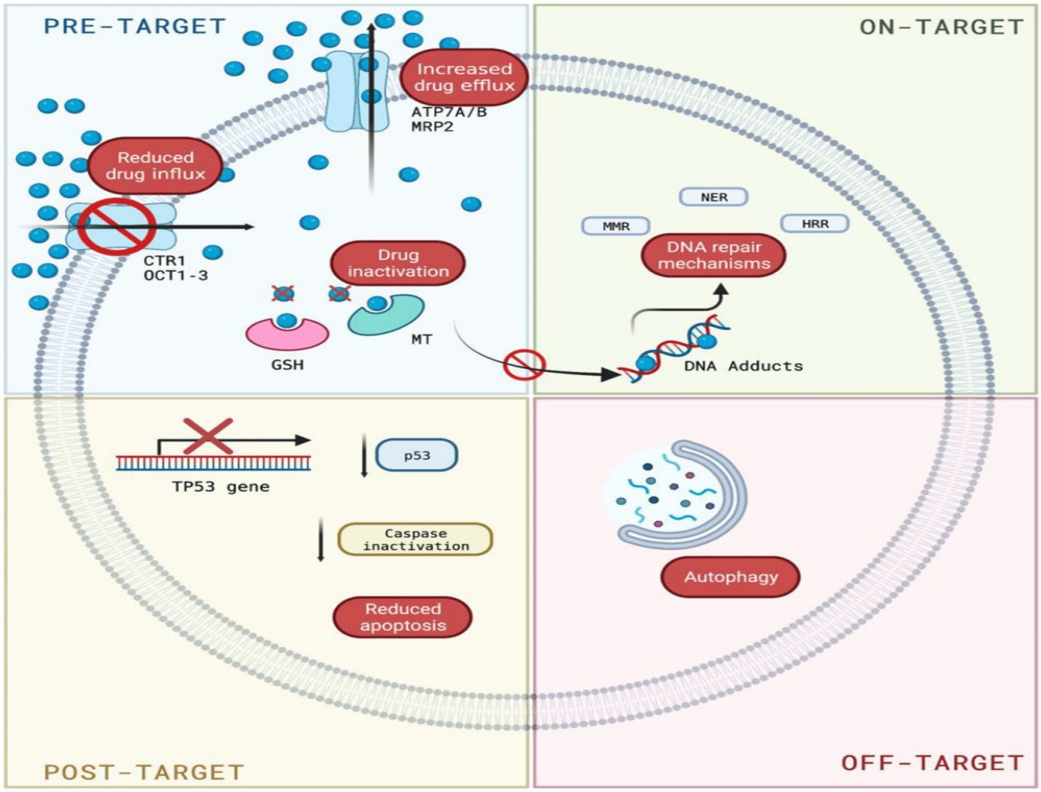

Figure 2. Illustration of the cisplatin mechanism of action in cancer treatment (accessed from Biorender.com 26 February 2024).

2.5 The role of epithelial-mesenchymal transition in cancer drug resistance

Numerous processes, including drug efflux, drug metabolism, and drug target mutations, can lead to treatment resistance. Cell-cell adhesions, apical-basal polarity, and the change to invasive mesenchymal cells are all part of epithelial- mesenchymal transition (EMT). EMT affects several biological and pathological processes, like wound healing, cancer cell metastasis, and drug resistance (Kim et al., 2017). Commonly, E-cadherin loss is what defines EMT. Gene expression changes brought about by EMT result in several phenotypic changes, including changes in cell shape, loss of cell adhesion, and acquiring characteristics unique to stem cells (Kim et al., 2017). A schematic representation of some of the properties that cell that undergo EMT acquire are summarized.

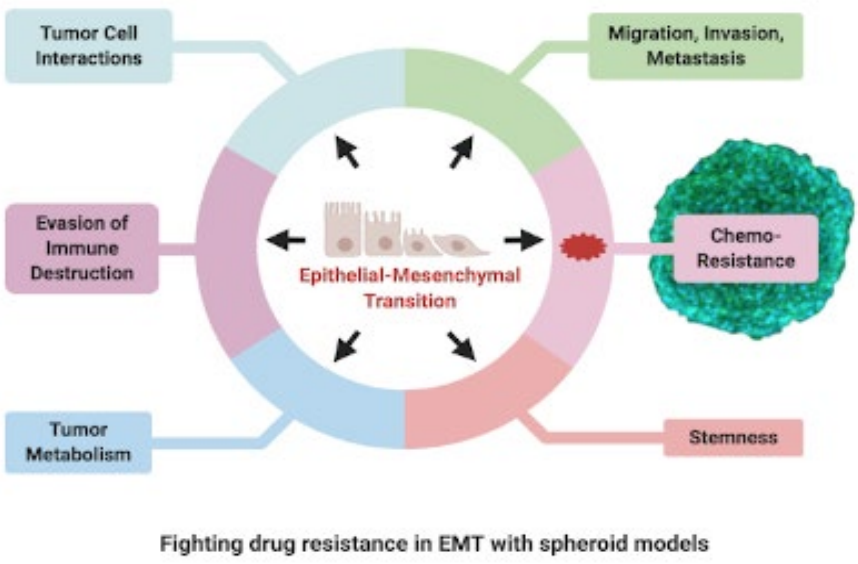

Figure 3. Epithelial-mesenchymal-transition MT results in phenotypic changes that lead to altered behaviour of the cells at the molecular level (LGC standard, Joe Lackey, 2024).

During the 1990s, researchers discovered a link between EMT and drug resistance in cancer cells. The studies demonstrated that the cancer cells resistant to drugs such as adriamycin and vinblastine underwent EMT and were characterized by decreased tight junctions and desmosomes and upregulated vimentin production (Ahmed et al., 2020). Currently, EMT is seen as a mechanism of drug resistance in various cancer types,

including pancreatic cancer, bladder cancer, and breast cancer (Hill and Wang, 2020). Cells that have undergone EMT reportedly display stem cell-like traits and have the same signalling pathways and drug resistance properties as those seen in cancer stem cells (CSCs) (Mani et al., 2008, Singh and Settleman, 2010).

Drug resistance in cancer stem cells is reported to be caused by the overexpression of cell membrane transporter proteins, which pump drugs out of the cells. These include the ABC transporters, multidrug-resistant gene-1, multidrug-resistance protein-1, and breast cancer-resistance protein (Fan et al., 2023). EMT upregulates these ABC transporters by binding the transcription factors to ABC transporter promoters, leading to drug resistance (Saxena et al., 2011).

2.6 The use of preclinical models in breast cancer studies

Cell culture and animal models have been used extensively in cancer research, focusing on the mechanisms of cancer cells and drug development. Most biomedical researchers use *in vitro* 2D culture models, forming a monolayer. Researchers currently use 2D cell cultures because of their high efficiency, simplicity, and inexpensive properties. However, during this technique, the ECM is not readily formed within the microenvironment, posing a limitation as cells require support from cellular and non-cellular structures, as reflected in the human body (Edmondson et al., 2014). New techniques that allow cells to assemble into 3D models and replicate cell-cell interactions *in vitro* provide power and advancement to cancer biology and drug discovery (Jubelin et al., 2022).

2.6.1 Animal studies in cancer research

As a model for researching cancer, rats assist researchers in understanding the complexities of how the body responds to treatment and the genetic mutations that can lead to cancer (Walrath et al., 2010). However, the development of these tumour animal models is complicated by unresolved technical challenges. Specifically, the transplantation methods are limited, and cancer cells are not engrafted with high

efficiency in transplants (Alghuwainem et al., 2019a). Xenograft tumours are superficially vascularized, and the stroma-tumour interactions are significantly limited (Idrisova et al., 2022) and in contrast to naturally occurring cancers, xenograft cancer models are significantly limited by the immune system deficiencies of the mice and rats used (Tian et al., 2020). Patient tumours usually exhibit intratumourally cellular and molecular heterogeneity, whereas xenografts are often derived from clones (Gerlinger et al., 2012, Zhang et al., 2014). Additionally, as opposed to most human tumours, where only a few cells actively divide at any given time, most xenograft cells are actively proliferating, which may explain why chemotherapeutic drugs that target dividing cells appear to be effective in xenograft models but have varying results in clinical stages (Simons and Brayton, 2017). As such, the restricted medicine administration and high-resolution imaging equipment requirements that result from the size differences between mice and humans pose a practical restriction in preclinical studies. Hence, allometric scaling and the inability of xenograft models to fully represent human TME and immune system interactions are some of the challenges of utilizing animal models in cancer research studies (Nair and Jacob, 2016). These limitations related to the cell line-based xenografts and animal models used as a host prompt for reviewing alternative methods to overcome these shortcomings and better recapitulate the human physiology and TME.

2.6.2 Two-dimensional vs Three-dimensional cell culture models in cancer studies

Cells have been cultured in 2D since the 1900s, which played an essential role in research but has been hampered by the inaccurate representation of tissue cells *in vitro* (Costa et al., 2016, Ferreira et al., 2018). Most drug screening is done in 2D *in vitro* cultures, which ignore the complexity of interactions seen in tumours *in vivo*. For instance, when cells are in 2D, they have more surface area in contact with the plastic and culture media than with other cells, causing them to polarize in ways that do not reflect physiological conditions (Baker and Chen, 2012). In the diagram below, some of the advantages and disadvantages of cells growing on the 2D and 3D scaffold models are outlined labelling each component.

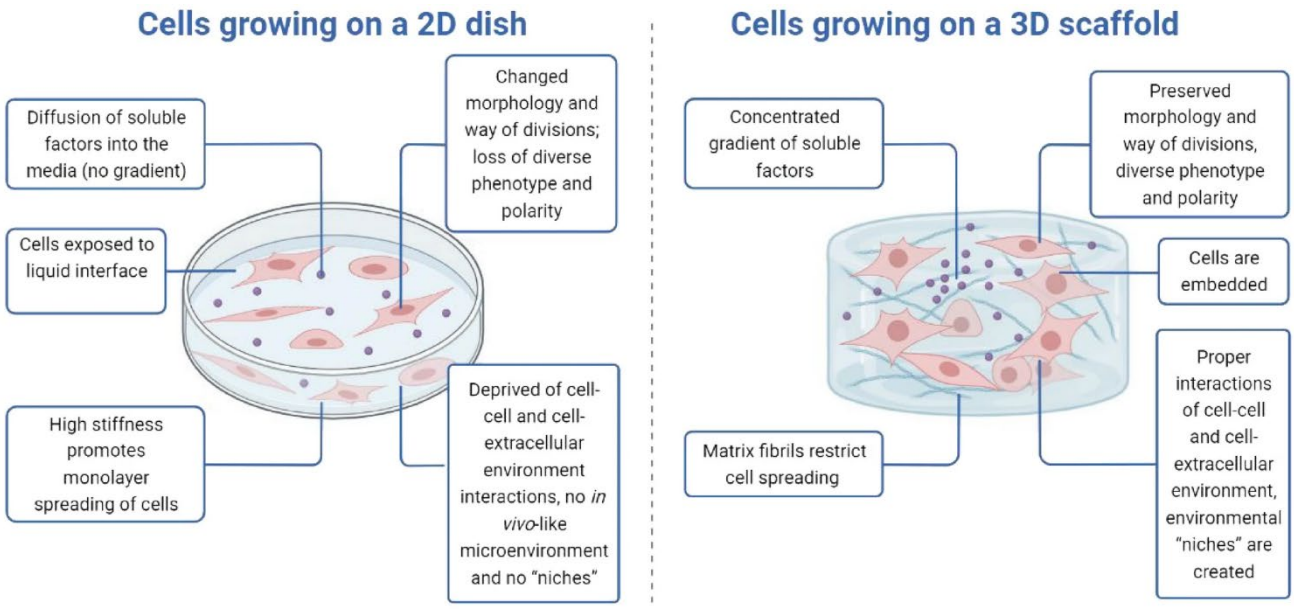

Figure 4. Differences of growing cells in a 2-D dish and 3D scaffolds (Owens, 2023).

In vitro models of human tumours are limited in their usefulness when cultivated in a 2D culture paradigm. Cancer, on the other hand, is a complicated heterotypic illness rooted in an organ along with its microenvironment, which means that many crucial characteristics of its *in vivo* equivalents are absent from the traditional 2D culture (Kenny et al., 2007).

Studies have been conducted to compare the traditional 2D and new 3D cell culturing methods. In a study by Fontoura et al. (2020), drug resistance, gene expression, and cell proliferation were examined in 2D and 3D cell culture models. Both models could support growth, but 3D models show morphologies closer to *in vivo* growth than monolayer models. Furthermore, following treatment, cells produced in all 3D culture systems showed at least 30% higher viability than the 2D group and exhibited greater resistance than those grown in monolayer.

A prior study evaluated drug sensitivity testing between 2D and 3D culture systems using three widely used anticancer medicines (docetaxel, cisplatin, and epirubicin) to treat TNBC. A scaffold-free culture was chosen because it is easy to use, highly reproducible, and uses the same culture conditions and cell viability assay as 2D culture. Compared to the 2D culture technique, the TNBC examined in this study showed superior resistance

to all three medications when tested in the 3D culture system. As a result, the 2D culture system might not be appropriate for anticancer drug sensitivity testing since the 3D culture more closely mimics an *in vivo* setting. However, it might be appropriate to test substances that damage DNA (Muguruma et al., 2020).

These results suggest that translational research is ideal for developing representative 3D cell culture systems that can effectively be used as standard *in vitro* models in research institutions.

2.7 The CelVivo ClinoStar™ system for spheroid generation

According to (Nolan et al., 2020), several well-established 3D models can be used to grow, maintain and characterize spheroids. A model of this kind is the Celvivo™ ClinoStar™ based rotating bioreactor developed by (Wrzesinski and Fey, 2015). A bioreactor refers to a device used to formulate 3D cultures of cells or tissues *in vitro* (Licata et al., 2023), characterized by its ability to regulate the environmental conditions, such as pH, dissolved gas concentration, flow rates, and nutrient supply in the system, removal of metabolic waste products and limiting excess shear stress (Vandermies and Fickers, 2019).

The ClinoStar™ system comprises ClinoReactors™ divided into two compartments, with the outer compartment responsible for humidification and gaseous exchange, while the inner compartment houses the cells and growth medium (van Niekerk et al., 2023). The ClinoReactors™ are fixed in a rotating ClinoStar™ system, which ensures that the cells self-aggregate without adhering to the surface of the ClinoReactor™ (Breslin and O'Driscoll, 2013).

Van Niekerk (2023) employed this ClinoStar™ system to construct a drug-resistant small lung cancer mini-tumour model, which was assessed for growth and viability for 28 days. After determining the experimental window, the model was evaluated for anticancer properties by administering irinotecan, paclitaxel, and cisplatin for 96 hours. The results suggested full functionality and viability of the 3D model throughout the characterization

period, and spheroids responded to treatment as of the model drugs, as seen *in vivo* (van Niekerk et al., 2023).

2.8 Spheroids as appropriate models for *in vitro* studies

The 3D cell culture platforms, when compared to 2D cultures, yield a more physiological cell-cell, cell-ECM architectural structure due to the scaffolds, hydrogels, and microfluidics. This renders 3D cellular models better for drug discovery tests, drug delivery, and toxicity (Haycock, 2011).

Spheroids are the simplest, most versatile structures characterized by their spherical aggregates of cancer cells that have self-assembled or encouraged by external factors to aggregate. The spheroids' structure, size, and appearance are usually influenced by factors, such as the cell line, the culture method, the seeding density, and shear stress (Tosca et al., 2023). Subsequently, larger spheroids display zones of proliferating cells on the outer layer, quiescent cells in the middle layer, and a necrotic core due to the limited diffusion of oxygen, nutrients, and metabolites (Mehta et al., 2012). This trend is commonly notable in the *in vivo* environment, whereby the peripheral cells are actively proliferating near the capillaries as their source of oxygen, while the inner cells are likely to die either by necrosis or apoptosis (Hirschhaeuser et al., 2010). Spheroid growth generally follows the S-shaped growth pattern, with the first phase of exponential growth followed by a time of linear growth and then a plateau (Han et al., 2021).

The strong cell-cell interactions displayed in spheroids are responsible for the behaviour of cancer cells, such as the proliferation rate, the survival, and the response of the cells to drugs. They increase the mass of the spheroids, creating a barrier that limits drug delivery into the core of the spheroids. These properties significantly affect the therapeutic effects of medication, increasing drug resistance and enhancing the reliability of drug screening in cancer spheroids (Nunes et al., 2019).

2.9 Established three-dimensional breast cancer models

Huang et al. (2020) established a TNBC MDA-MB-231 spheroid model to investigate malignant cells and tumour development and to assess drug resistance. As opposed to 2D monolayer cultures, breast cancer spheroids can replicate the complex *in vivo* TME better. To generate the MDA-MB-231 spheroids, the microwell array method was employed. In this scaffold-based technique, cells are collected to the bottom of the plate by the sidewalls, eventually encouraging the clumping up of the cells to form spheroids. The proteins associated with EMT were investigated using the western blot assay in conjunction with confocal microscopy. The IC_{50} of carboplatin and doxorubicin was reported to measure the drug resistance of these spheroids. As a result of this study, simple spheroids were developed, and their structure, growth, and proliferation characteristics were demonstrated. According to their findings, the spheroids exhibited superior EMT and were more resistant to toxicological responses when compared with conventional 2D cultures.

In another study, a 3D culture system examined multidrug resistance in breast cancer (Ding et al., 2018). A 3D silk scaffolds were employed to culture the breast cancer MCF-7 cell line to characterize the growth properties, morphology, and gene/protein expression. The use of the scaffold method to develop a 3D microenvironment displayed the ability of the cells to extend the proliferation stage effectively, the overexpression of MDR-related gene proteins, and upregulate chemoresistance *in vitro*. The study's results highlighted that the breast cancer cells cultured in a 3D environment displayed a modification in their cell cycle, as well as an increased proportion of cells that exhibited properties seen in breast cancer stem cells (BCSCs). This model can potentially enhance the comprehension of tumour multidrug resistance (MDR) more precisely and systematically.

These studies suggest that developing and characterizing a 3D cell model with relevant properties could be valuable for studying drug efficacy in preclinical facilities and developing anticancer compounds that bypass chemo-resistant mechanisms.

2.6.3 Three-dimensional culture techniques

Two unique categories can be formulated from cell culture techniques and protocols created to culture cells in 3D environments *in vitro*, namely scaffold-based and scaffold-free.

2.6.3.1 Scaffold-based techniques

Growing cells on a structural scaffold replicating the natural ECM using biopolymers is the most traditional method for 3D cell culture. These scaffolds can be used in regular cell culture processes or as the basis for more challenging tissue engineering initiatives, such as creating artificial organs. In scaffold-based 3D cell culture, cells are cultured on a scaffold, where they connect and populate (Alghuwainem et al., 2019a). These scaffolds are made of biomaterials that allow for enough gaseous exchange, nutrient availability, and growth factors supply. One example is a polymeric rigid material-based support where the cells are grown alongside sponge-like structures or threads (Tosca et al., 2023). The biomaterials used to culture cells are synthetic or naturally derived polymers, which provide support for cell growth and mimic ECM conditions. Cells can either be only surface-coated or anchored in the hydrogels. Hydrogels can be divided into a few categories with various unique features depending on the type of polymer used. These groups consist of ECM protein-based, synthetic, and natural hydrogels (Chen et al., 2023).

Natural Hydrogels are based on chains of covalently or non-covalently bound hydrophilic polymers. Natural or synthetic polymers produce gels when crosslinked by covalent or noncovalent bonding. Alginate, gelatine, hyaluronic acid, agarose, laminin, collagen (Jensen and Teng, 2020, Liu et al., 2022) or fibrin are examples of bioactive and biodegradable natural polymers, which can be categorized as proteins, polysaccharides, or polynucleotides. Additionally, Unlike gels, hydrogels are more solid than liquid and can absorb large amounts of water and swell without disintegrating (Nikolova and Chavali, 2019).

Biological tissues and processes can be adapted to hydrogels. These scaffolds mimic ECM and have tissue-like stiffness, enabling factors like cytokines and growth factors to move through them (Langhans, 2018). However, scaffolds based solely on natural hydrogels cannot hold their 3D shape because of their poor mechanical properties (Nikolova and Chavali, 2019). The properties of **synthetic hydrogels** make them more consistent, reproducible, and customizable compared to natural hydrogels (Habanjar et al., 2021). Despite their hydrophobicity, synthetic polymers do not display high cell affinity due to the lack of cell recognition sites (Nikolova and Chavali, 2019).

Choosing a reliable scaffold to use in research is crucial. The stiffness of the scaffold can negatively impact cancer progression and treatment resistance; therefore, taking these parameters into account helps to ensure that the most appropriate scaffold is employed. It also affects cell behaviour, which could be detrimental to disease modelling. Additionally, the ECM's functionality will influence how cells are supported and interact, changing how cells behave. To acquire the optimum match for the cell type, it is necessary to specify and optimize the capabilities of the selected scaffold. Some of the commonly used 3D based scaffolds in cancer can be seen in the illustration below.

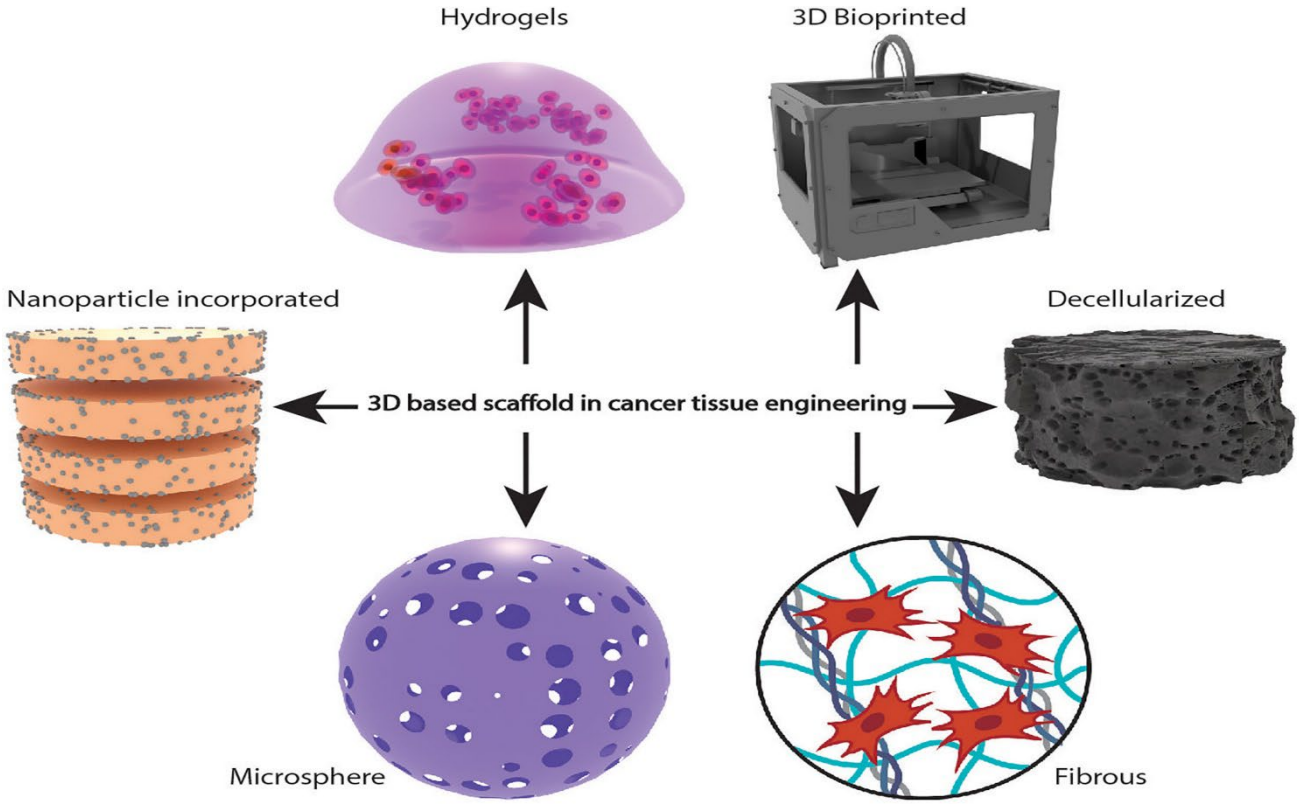

Figure 5. Example of the scaffold-based 3D techniques in cancer research (Unnikrishnan et al., 2021).

2.6.3.2 Scaffold-free technique

A scaffold-free approach involves building a scaffold with single cells, cell aggregates, or tissue strands. It is dependent on the building blocks' inherent ability to be combined and built into larger structures (Ovsianikov et al., 2018). Unlike the scaffold-based technique, cell proliferation and migration are not decisive factors in this method. As a result, tissue construction can be completed in a shorter time (Ovsianikov et al., 2018). The definition of a scaffold-free structure is still ambiguous and debatable, however, the commonly used definition is the development of a living tissue using single cells that further determine the architecture and matrix components (Alghuwainem et al., 2019b). According to Athanasiou et al., "scaffold-less tissue engineering refers to any platform that does not require cell seeding or adherence within an exogenous, 3D material" (Athanasiou et al., 2013). Generally, when cells are confluent, they can produce large amounts of ECM. This feature was investigated using cells treated with growth factors and matured in a mould to develop scaffold-free 3D models that produce their own matrix (Miyazaki et al., 2010).

The basis of a scaffold-free technique is further characterized by the cell organization and self-assembly by natural features to allow cells to perform events with minimal interference, such as the development of spheroids (Athanasiou et al., 2013). Using this method, the cells are solemnly let to self-aggregate into unattached spheroids. These spheroids then organize and form their ECM, like solid *in vivo* tumours indicating sufficient nutrient supply. Spheroids in this technique usually have a constant size and shape, rendering them superior *in vitro* cellular models for high-throughput screening (Mehta et al., 2012).

The most common examples of scaffold-free techniques include low attachment plates, the hanging drop method, 3D petri dishes, and 3D bioreactors.

- For the **low attachment plate method**, wells are coated with a polymer to reduce adhesion. After centrifugation, well plates are filled with a cell suspension to create spheroids (Breslin & O'Driscoll, 2016).
- During the **hanging drop method**, a suspension aliquot of cells is agglomerated in microarrays and fabricated into droplets containing spheroids. Spheroid size can be manipulated by adjusting the cell suspension's density (Ryu et al., 2019).
- Utilizing a bioreactor that is constantly moving, **agitation-based methods** recreate microgravity. Continual swirling in a cell suspension progressively transforms solitary cells into aggregates that cannot attach to the container wall. Thus, non-uniform spheroids are produced randomly (Ryu et al., 2019). An essential advantage of rotating reactors is efficient gas and nutrient exchange inside the bioreactors (Wrzesinski and Fey, 2018). In addition, a variety of benefits of this method include its simplicity, extensive production of 3D cultures, and extended culture of 3D spheroids (Barrila et al., 2010). The disadvantage to rotating bioreactors is that they require specialized equipment that is relatively expensive, as well as high quality/quantity of culture medium (Barrila et al., 2010). In the image below techniques that are used to generate scaffold-free 3D models are shown.

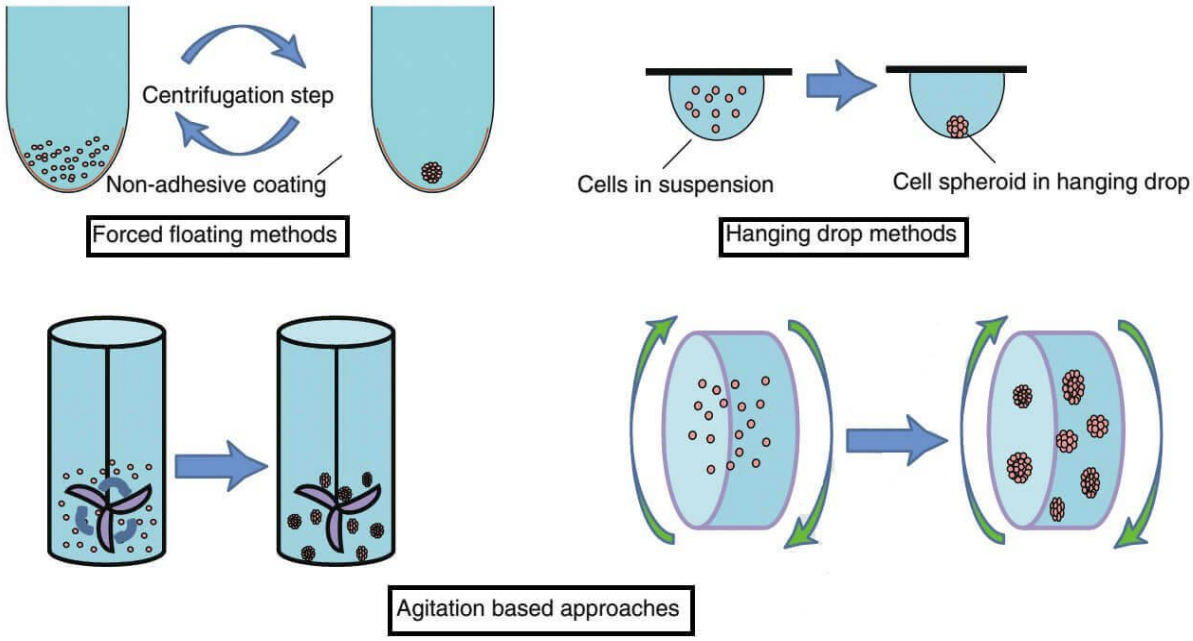

Figure 6. A visual illustration of the different techniques employed to generate scaffold-free 3D models (Adams et al., 2023).

CHAPTER 3 – METHODOLOGY

3.1 Materials and Methods

Site selection: The research experiments for this research study were executed at two locations: The Basic Medical Sciences department at the University of the Free State in Bloemfontein and the Centre of Excellence for Pharmaceutical Sciences (Pharmacen™) at the North-West University in Potchefstroom.

The MDA-MB-231 (HTB-26™) cell line was sourced from the American Tissue Culture Collection (ATCC) through Industrial Analytical [Pty] Ltd, which forms part of LGC standards, the sole supplier of ATCC materials in South Africa. The MDA-MB-321 cell line was derived from a pleural effusion of a patient with breast cancer, and the model was described as TNBC due to the absence of the ER, PR, and HER2 and the high rate of recurrence. The importation of the cells as biological material in terms of section 68 of the National Health Act 2003 (Act No. 61 of 2003) was handled by Industrial Analytical [Pty] Ltd, including the subsequent customs clearance and shipment of materials using cold chain handling to the Basic Medical Sciences department at the University of the Free State. The MDA-MB-231-HTB-26™ cell line is identified as a non-hazardous substance or mixture (BSL-1) according to the United States Occupational Safety and Health Administration (OSHA) Hazard Communication Standard (29 CFR 1910.1200) and was handled as a non-hazardous material using aseptic techniques which were observed by all personnel working in the lab.

In addition to the cell line, the following consumables were utilized in this project to carry out experiments and maintain cell growth: Phosphate-buffered saline (PBS), Trypsin-EDTA 0,5%, and Foetal Bovine serum (FBS) purchased from Thermo Fisher Scientific, Johannesburg, South Africa. Gibco High Glucose Dulbecco's modified eagle medium (DMEM) and Penicillin-streptomycin were purchased from Thermo Fisher Scientific, Johannesburg, South Africa. The CellTiter™-Glo Luminescent buffer was purchased from Promega. The ATP standard for the intracellular ATP assay was

purchased from Sigma-Aldrich, Johannesburg, South Africa, as well as the assay buffer and AK detection reagent from Lonza (Whitehead Scientific [Pty] Ltd., Cape Town, South Africa). Lysis buffer was prepared in the laboratory. Bovine serum albumin (BSA) and colour reagent used in the soluble protein assay from Bio-Rad Laboratories (Pty) Ltd, South Africa.

3.2 Culture and maintenance of MDA-MB-231 cells

The TNBC MDA-MB-231 cell line was cultured in a T25 flask inside a sterile Airtech laminar flow hood. Frozen 2 mL vials of the cell line were suspended in warmed DMEM culture medium supplemented with 10% FBS and 1% penicillin-streptomycin and cultured as monolayer cultures at 37°C in a 5% CO_2 and 95% humidified air incubator. Cells were grown to 80% confluency, washed with PBS, detached using trypsin, and a cell count was done using an automated cell counter TC20. Following the cell count, 1 mL cell suspension was seeded into T75 flasks containing 9 mL complete medium.

Trypsinization:

Cells were removed from the incubator and observed under a microscope for confluency. Following confirmation of 80% confluency, the culture flasks containing cells were placed inside the laminar flow hood, the DMEM was removed, and cells were rinsed three times with 5 mL pre-warmed PBS to ensure no trace of the spent DMEM. To dissociate the cells from the base of the culture flask, 3 mL of trypsin was added to the culture flask and incubated for 10 min to allow catalysis of adherent proteins and detach the monolayer. Once 10 min. has elapsed, the cells are observed under the microscope to assess if the monolayer has been detached from the culture flask surface. To counteract and neutralize the effects of trypsin, cells were re-suspended in pre-warmed 10 mL DMEM and transferred into a 15 mL conical tube, and this cell suspension was centrifuged at 2000 rpm for 10 min. at room temperature. The supernatant was extracted following centrifugation, and cells were resuspended in 2 mL of DMEM. Gentle pipetting is used to break down the pellet and mix it properly with the culture medium to

prepare for cell count. For the count, 20 µl of the cell suspension and 20 µl of trypan blue dye were added in an Eppendorf tube. Following this, 10 µl of the mixture is transferred onto a cell counter slide and inserted into the TC20 automated cell counter to determine the number of live cells. Following this, the cells were either seeded into 2 new culture flasks or seeded into the 96-well plate for the 3-(4,5-dimethylthiazol-2-yl)-2,5-diphenyltetrazolium bromide (MTT) experiment.

3.3 Induction of cisplatin resistance

This study established 2D cisplatin-resistant MDA-MB-231 cells by repeatedly exposing a Wild-type/Parental MDA-MB-231 cell population to a chemotherapeutic drug (cisplatin) in culture. Firstly, the Wild-type/Parental MDA-MB-231 cells were cultured with a seeding density of 10,000 cells/well in a 96-well plate (n=6) with media supplemented with cisplatin (0.01-10 µM) for 48 h. The IC_{50} (drug concentration causing 50% growth inhibition) was determined as described in section 3.3.2. Thereafter, the remaining survival cells were continuously exposed to IC_{10}-IC_{50} drug concentration treatment for 48 h alternating a recovery period of 48 h for approximately nine months to induce cisplatin resistance in the cells. Drug resistant cell models are typically developed *in vitro* by exposing cancer cells to chemotherapy agents over 3-8 months, depending on factors such as parent cell line, drug concentration and treatment frequency (McDermott et al., 2014b). Thus, a similar method was adapted in this study to acquire resistance. To confirm resistance in the exposed variant of MDA-MB-231 cells, the MTT assay was performed, where after the IC_{50} of the Wild-type/Parental MDA-MB-231 and cisplatin-resistant MDA-MB-231 cells were used to determine the fold-resistance.

3.3.1 Preparation of the cisplatin

The cisplatin stock treatment was prepared by weighing 12 mg of cisplatin powder (Sigma-Aldrich) and dissolving it in 6 mL of sodium chloride solution (saline) in a 15 mL conical tube. This resulted in a stock concentration of 6×10^3 µM, and from this stock

solution, the desired treatment concentrations were calculated and added to the DMEM and used for the treatment period.

3.3.2 A 3-(4,5-Dimethylthiazol-2-yl)-2,5-diphenyltetrazolium bromide cytotoxicity assay

The basis for the MTT assay is the reduction of yellow soluble MTT reagent into insoluble purple formazan crystals by the metabolically active cells (Nga et al., 2020).

The WT/Parental and the cisplatin-exposed MDA-MB-231 cells were cultured with a seeding density of 10,000 cells/well in separate 96-well plates (n=6) and were incubated to allow for attachment overnight. Following this, cells were treated with cisplatin serial dilution concentrations (0.01, 0.1, 1, 10, and 100 µM); an untreated control and no cells control were also grouped. 100 µl of DMEM with treatment was added to each well and then incubated for 48 h. After incubation with treatment, the treatment was removed from each well, and the cells were rinsed with 100 µl PBS. Each well was filled with 100 µl of DMEM and 20 µl of concentration 0.5 mg/mL of MTT reagent. The plates were then incubated at 37ºC for 4 h. Following the incubation, the media with MTT solution was discarded, and 50 µl DMSO was added to each well. The plates were placed on a shaker for 25 min at room temperature. Once the formazan crystals had dissolved, absorbance was measured at 570 nm relative to the 630 nm wavelength on a Promega GloMax® Discover microplate reader. For these paired cell lines, the IC_{50} (drug concentration causing 50% growth inhibition relative to untreated control) was utilized to calculate the fold resistance or increase in resistance using the following formula (McDermott et al., 2014a): *Fold resistance = IC_{50} of cisplatin-resistant cell line/IC_{50} of parental cell line*.

3.4 Spheroid establishment and maintenance

The ClinoStar™ system (CelVivo ApS, Odense, Denmark) was used to develop and maintain a novel cisplatin-resistant MDA-MB-231 TNBC spheroid model. The ClinoStar™ system comprises six engines, rotating ClinoReactors™ with adjustable rotation speeds, and an incubation chamber with temperature maintained at 37ºC and 5%

CO_2. The cisplatin-resistant MDA-MB-231 spheroids were generated using the protocol by Wrzesinski et al. 2013 previously described methods (Wrzesinski and Fey, 2013)

3.4.1 Preparation of a cell suspension

The resistant MDA-MB-231 cells were grown under flat culture conditions until 80% confluence. After trypsinization (4 minutes), the cell suspension was centrifuged at 204 x g for 5 min. The supernatant was disposed of, and the cell pellet was resuspended in 5 ml media. Cell counting was done using the Sceptre handheld automated cell counter.

3.4.2 Initiation of spheroids

Four ClinoReactors™ were set up for the model establishment of the cisplatin-resistant MDA-MB-231 spheroids. ClinoReactors™ were prepared by hydrating the humidification beads by adding 25 mL of sterile water in the hydration port and 6 mL of PBS in the cell chamber. The ClinoReactor™ was incubated for 6 h in the ClinoStar™ with slow rotation. The PBS was discarded, and the chamber was filled with media. The ClinoReactor™ was closed and placed into the ClinoStar™, rotating at 15 rpm overnight to allow equilibration. After equilibration, 800,000 cells were inserted into ClinoReactor™. The ClinoReactors™ were filled to 10 mL with culture medium containing 0.5 µg/mL ascorbic acid, closed, and placed into the ClinoStar™, rotating at 2.5 rpm overnight. To achieve optimal growth conditions, the growth medium was exchanged every 48 h, and the speed of rotation was adjusted to compensate for the spheroids' growth. On day 2 (48 h in culture), the contents in each ClinoReactor™ were divided (1:2) into two ClinoReactors™, resulting in eight ClinoReactor™ with media containing 0.5 ug/mL ascorbic acid. This was to minimize clumping of the single-cell suspension and assist with spheroid formation. On day 4 in culture, the media was exchanged, but ascorbic acid was removed, and the media was supplemented with 20% FBS. Prolonged use of ascorbic acid can result in clumping of the cells. The increase in FBS concentration assisted with compactness and growth of the spheroids. The formed spheroids in each ClinoReactor™ were sorted on day 6 of culture, and 180 spheroids were placed into each ClinoReactor™ for characterization. Microscopy was used to

examine spheroid integrity and diameter throughout the experiment, utilizing an A DFK 72AUCO2 USB 2.0 colour industrial camera (The Imaging Source, Bremen, Germany) linked to an inverted microscope (Nikon TS100/TS100F, Nikon instruments, Tokyo) and the Axio Vert A1 inverted transmitted light microscopy with AxioCam 305 mono fitted camera (195-043518) (Zeiss, Johannesburg, South Africa).

3.4.3 Resistant MDA-MB-231 spheroid model characterization

The spheroids were characterized every second day until day 28, from day 6 in culture. This was done to assess the spheroids' health and growth and to identify the period where the spheroids reached a metabolic equilibrium or the optimal experimental window of the model. Characterization was performed using two biological groups (each consisting of two ClinoReactors™), and sampling was alternated between the two ClinoReactor™ per biological group to avoid the spheroid population decreasing too fast. Three technical replicates were sampled from each biological group every 48 h. This resulted in six samples for each parameter (n = 6).

3.4.3.1 Soluble protein content

The soluble protein content can indicate the growth of the spheroids and was determined using a Bradford assay. BSA (2 mg/mL, Bio-Rad, Lasec SA (Pty) Ltd., Midrand, South Africa) was diluted in water to create a reference standard curve. On days 6 and 8 of culture, 3 spheroids were sampled from each designated ClinoReactor™, and 1 spheroid was placed per well of a clear flat-bottomed 96-well plate containing 150 µl PBS. A DFK 72AUCO2 USB 2.0 colour industrial camera (The Imaging Source, Bremen, Germany) linked to an inverted microscope (Nikon TS100/TS100F, Nikon instruments, Tokyo) and the Axio Vert A1 inverted transmitted light microscopy with AxioCam 305 mono fitted camera (195-043518) (Zeiss, Johannesburg, South Africa) was utilized to take photomicrographs of the spheroids. Following imaging, the PBS was removed, and 150 µl of distilled water was added to each well, followed by 10 µl lysis buffer. The cells were pipetted to lyse all components of the spheroids, followed by the addition of a 40 µl colour agent, making up the volume of 200 µl. From Day 10, three spheroids were sampled from each ClinoReactor™; protein samples had to be diluted 1:1 on days 10,

12, 14, and 16, and the samples thereafter were not diluted. The 96-well plate was then incubated at room temperature for 5 min. Absorbance was assessed on a SpectraMax™ Paradigm® plate reader (Molecular Devices Inc, Separations, Randburg, South Africa) at a wavelength of 595 nm.

3.4.3.2 Intracellular adenosine triphosphate assay

The generation of ATP was used to determine the viability of cells. According to the manufacturer's guidelines, the CellTiter-Glo® Luminescent Cell Viability Assay and ATP standard were utilized to measure the amount of ATP the cells generated, signifying their metabolic activity. Every 48 h, 3 spheroids were removed randomly from each of the relevant ClinoReator™ and transferred to a black clear-bottomed 96-well plate and imaged. The excess medium was removed from the wells using a pipette, adding a 100 µl volume of PBS and 100 µl CellTiter-Glo luminescent lysis buffer. Gentle repetitive pipetting was used to facilitate the lysis of the spheroids in each well. The plate was covered with tin foil to shield it from light and placed onto a table shaker for 40 min at 300 rpm. Using a SpectraMax® Paradigm® plate reader, luminescence was measured. The samples were expressed as an average ATP content (µM) per spheroid, normalized per µg soluble protein, and measured in relation to a known ATP standard.

3.4.3.3 Planimetric determination

A DFK 72AUCO2 USB 2.0 colour industrial camera (The Imaging Source, Bremen, Germany) linked to an inverted microscope (Nikon TS100/TS100F, Nikon instruments, Tokyo) and the Axio Vert A1 inverted transmitted light microscopy with AxioCam 305 mono fitted camera (195-043518) (Zeiss, Johannesburg, South Africa) was utilized to capture the photomicrographs of the spheroids at the various time points were used for planimetric measurements as an indicator of spheroid growth. These photomicrographs were moved to the Image J software, which measured the surface area of each spheroid in μm^2.

3.4.3.4 Extracellular adenylate kinase assay

AK is a phosphotransferase enzyme that maintains cell energy. When AK is released from eukaryotic cells, it indicates cell death and toxicity. The ToxiLight™ BioAssay kit was used in a non-destructive assay, and healthy cells were not damaged daily to assess for AK release. After sampling, before media exchange, a 200 µl sample was withdrawn from the spheroid culture medium and centrifuged for 5 min at 140 x g. Then, 160 µl of the supernatant was withdrawn and transferred into a new microcentrifuge tube and centrifuged at 15 000 x g for 15 min. Of the supernatant, 140 µl was transferred to new tubes, snap-frozen using liquid nitrogen, and kept at -80°C until use. The samples were defrosted, and 20 µl samples were placed in a black 96-well plate in triplicate. A standard curve prepared from a known concentration of dead MDA- MB 231 cells was included in triplicate, where each sample contained 20 µl. AK detection reagent (100 µl) was added to each well containing the experimental and standard curve samples. Gentle pipetting ensured that the reagent and the medium were adequately mixed. The plate was then covered and incubated for 20 min on a shaker at room temperature. The luminescence was measured on a SpectraMax® Paradigm plate reader in the same manner as explained for the ATP assay. The number of dead cells per mL of media was obtained by quantifying AK in relation to a recognized dead cell standard. As the volume per ClinoReactor™ was 10 mL, the AK was multiplied by 10 and then normalized to the soluble protein content.

3.4.3.5 Approximate glucose consumption assay

20 µl of the spent cell culture medium was removed from the designated ClinoReators™ and transferred into a microcentrifuge tube before medium exchange. A OneTouch™ Vita glucose monitor and corresponding test strips (LifeScan Europe, Zug, Switzerland) were used to measure the glucose quantity in the medium. To determine the triplicate glucose concentrations (mmol/L), the spent medium was placed onto the test strips (10 µl). The fresh medium's glucose concentration was also tested in triplicate before being added to the ClinoReactor™. The result was 21.23 mmol/L, the highest starting glucose content in a ClinoReactor™. To calculate the approximate amount of glucose consumed,

the glucose content of the fresh medium was subtracted from the glucose content of the spent medium. To ensure reproducibility, this was divided by the total soluble protein present in each ClinoReactor™ to calculate the approximate glucose consumption per protein (µg) in triplicate. This assay indicates approximate glucose consumption and, thus, metabolic activity of the spheroids. As the cells die, less glucose is consumed from the growth medium.

3.5 Qualification of the three-dimensional cisplatin-resistant MDA-MB-231 spheroid model

The response of the cisplatin-resistant MDA-MB-231 spheroids to treatment was assessed using two common chemotherapeutic agents: doxorubicin hydrochloride (Sigma-Aldrich) and cisplatin (Sigma-Aldrich). The ClinoReactors™ setup and upkeep followed a similar protocol to that of characterization. On day 6 of spheroid culturing, 180 spheroids were placed into each ClinoReactor™ and maintained. On day 10 of culture, spheroids were sorted again, and 100 spheroids were sorted and inserted into each ClinoReactor™ (two ClinoReactors™ per treatment group) in order to prepare them for treatment. On day 12 (0 h), treatment was initiated for 96 h, with sampling every 24 h. Every 24 hours following sampling, the drug-containing medium with 20% FBS was changed, and the daily drug dosage was modified based on the residual estimated spheroid biomass per ClinoReactor™. Sampled spheroids were observed at 0 h and at each time point post-treatment to observe any changes in structure and size relative to the untreated control group. Assays were performed as described in Section (3.4.3).

3.5.1 Treatment calculation

After sampling from each ClinoReactor™ daily, the spheroids' biomass obtained from the soluble protein content was calculated to estimate the daily dosages of the two chemotherapeutic medications. These dosages were then modified based on each chemotherapy dose. The soluble protein content (µg) per spheroid and the number of

spheroids left in each ClinoReactor™ each day were multiplied to determine the total protein content (µg) per bioreactor. Subsequently, the dosages of doxorubicin and cisplatin were adjusted. This ensured that the spheroids were consistently administered the same treatment dose during the experiment. Doxorubicin stock treatment for the treatment experiment of the spheroids was prepared by dissolving 5 mg of doxorubicin compound in 0.5 mL of DMSO. This was stored as 30 µl in Eppendorf tubes. Cisplatin was prepared as described in section 3.3.1

After sampling for each assay, the medium in the bioreactors was replaced with the medium containing the previous day's treatment. Following the measurement of each bioreactor's protein soluble content, a new treatment dose was calculated and prepared, and each bioreactor's medium was changed out for a new one containing the new treatment. The therapeutic dosages used for patients with TNBC served as the basis for the treatment dosages in this study, cisplatin (25 mg/m^2), and doxorubicin (60mg/m^2). In addition to the clinical doses, an IC_{50} dose of cisplatin was also used based on the MTT assay data of the 2D-resistant MDA-MB-231 cell culture. The treatment groups were categorized as untreated control, cisplatin clinical dose (4,435 x 10^{-6} µg cisplatin/µg protein), doxorubicin clinical dose (1,064 x 10^{-5} µg doxorubicin/µg protein) and cisplatin IC_{50} (8,06 x 10^{-2} µg cisplatin/µg protein).

3.6 Statistical Analysis

Through the use of GraphPad Prism's three-parameter logistic equation, the best-fit IC_{50} values and corresponding 95% confidence intervals were obtained through non-linear regression analysis of sigmoid aldose-response curves (GraphPad Prism version 10.2.3 for Windows, GraphPad Software, San Diego, California, USA, http://www.graphpad.com). One-way analysis of variance (ANOVA) was used to determine the P-values, which were then calculated using GraphPad. Dunnett's method was used for all pairwise multiple comparisons, and 0.05 ($p<0.05$) was chosen as the overall significant threshold.

3.7 Ethical consideration

This research protocol was submitted and approved by the Environmental and Biosafety Research Ethics Committee (EBREC) at the University of the Free State (UFS-ESD2023/0001/23), as well as the Research Ethics Committee (REC) at the North-West University.

CHAPTER 4 – RESULTS

4.1 Induction of cisplatin-resistance

This study developed 2D cisplatin-resistant MDA-MB-231 cells by repeatedly exposing cancer cells to a chemotherapeutic drug. In culture, the cells were continuously passaged until they reached optimal growth. Following this, the MDA-MB-231 cells were cultured in a medium supplemented with cisplatin treatment (0.01-10 μM) for 48 h and another 48 h of recovery (fresh culture media without treatment) for nine months to induce cisplatin resistance in the cells.

The growth inhibitory effect of cisplatin on the 2D MDA-MB-231 wild-type (WT)/Parental cell cultures was first investigated (Figure 7A) using the MTT assay. Then, the MDA-MB-231 WT-dose response curve was used to determine the drug concentrations required to reduce the culture's viability by 10% and 50% (IC_{10} and IC_{50}) in the process of developing a cisplatin-resistant MDA-MB-231 cell population. After resistance induction, the IC_{50} of the cisplatin-resistant MDA-MB-231 cells was determined using the MTT assay (Figure 7B). The IC_{50} of the MDA-MB-231 WT/Parental (8,06 μM) was compared to the IC_{50} of the cisplatin-resistant MDA-MB-231 cells (26,73 μM) to determine the fold resistance.

Fold resistance = IC_{50} of resistant cell /IC_{50} of WT cell line

= 26,73 μM/8,06 μM

= 3,32

The inhibitory concentrations reveal that the IC_{50} of the cisplatin-resistant MDA-MB-231 cells was three-fold higher than the IC_{50} value obtained for the WT/Parental MDA-MB-231 cells.

A B

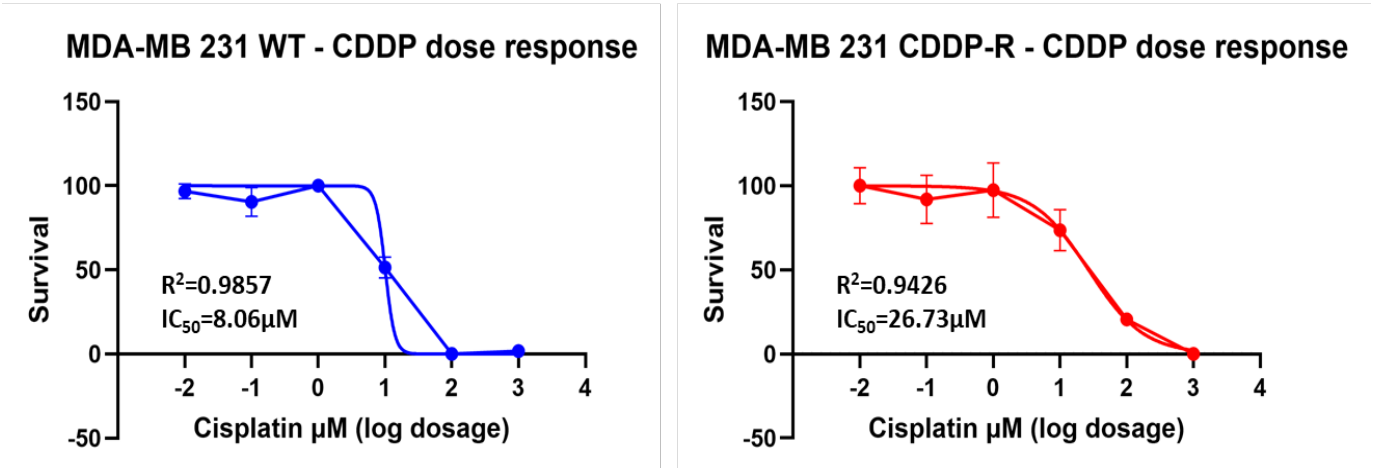

Figure 7. Dose-response effect of cisplatin on the cellular viability of 2D WT and cisplatin-resistant MDA-MB-231 cells. (A) Dose-response curve of WT MDA-MB-231 and 50% inhibitory concentration of cisplatin (IC_{50}=8.06 µM) after a 48 h treatment. (B) Dose-response curve of cisplatin-resistant MDA-MB-231 cells and 50% inhibitory concentration of cisplatin (IC_{50}=26.73 µM following a 48 h treatment.

4.2 Characterization of the cisplatin-resistant MDA-MB-231 spheroid model

The cisplatin-resistant MDA-MB-231 spheroids were initiated as a single-cell suspension in the ClinoReactors™ on day 0. From day 6 until day 28, the planimetry, soluble protein content, intracellular ATP content, extracellular AK released, and approximate glucose intake were used to measure and analyze the spheroids' health and growth.

Figure 8. The CelVivo™ ClinoStar™ System, with the ClinoReactors™, used for culturing spheroids in a growth medium. An internet-connected device controls the system's conditions, such as temperature range, carbon dioxide levels, and rotation speed. It visualizes the growing spheroids without opening the system and retrieving the ClinoReactors™ (Taken from the CelVivo™ website, 21 June 2024).

4.2.1 Planimetric measurements

The physical growth and shape of the cisplatin-resistant MDA-MB-231 spheroids are depicted in Figure 9 from day 6 until the end of the 28-day characterization period. Upon observation, the spheroids steadily maintained a specific size (20 000 μm^2) and shape and seemed to become more compact from day 6 to day 20. After that, from day 24, the spheroids disintegrated, became fragile, and decreased in size at day 26. On days 12, 18, and 22 the spheroids were not captured, this was to minimize the period of time where they are placed on the surface as this proved to disturb the spheroids greatly. As a

measure of spheroid size and growth, the planar surface area of the cisplatin-MDA-MB-231 spheroids was plotted as a function of time and is displayed in Figure 10 (A).

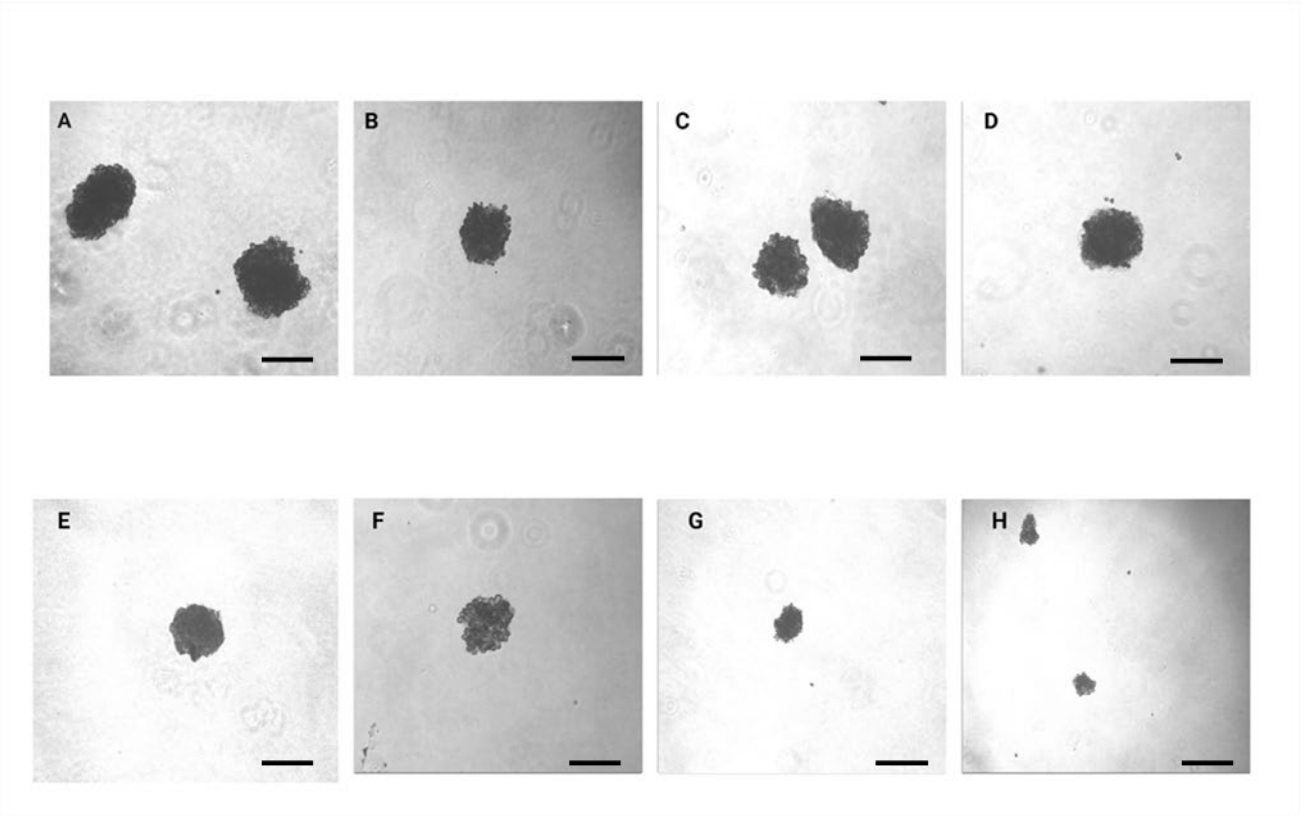

Figure 9. Photomicrographs of the cisplatin-resistant MDA-MB-231 spheroids cultured in ClinoReactors™ as observed on (A) day 6, (B) day 8, (C) day 10, (D) day 14, (E) day 16, (F) day 20, (G) day 24, and (H) day 26 of culture (4x magnification; scale bars = 200 µm).

4.2.2 Soluble protein content

Each experimental ClinoReactor™ was filled with 180 spheroids on day 6, and every two days, the amount of soluble protein was determined. Figure 10 (B) displays each spheroid's soluble protein content as a function of time till day 28. The soluble protein content results demonstrated a decrease between days 6 and 10, possibly due to handling during the sorting of the spheroids or because the cells were still adapting to the new 3D environment. The protein content then recovered to day 12. The protein content remained stable from day 12 to day 22, suggesting consistent viability, although no significant growth was observed. After day 22, some fluctuation was noted till the end of

characterization. During these days, there were size variations as the spheroids lost integrity.

4.2.3 Intracellular ATP content

The intracellular ATP/protein content for cisplatin MDA-MB-231 spheroids, as seen in Figure 10 (C), was expressed in terms of protein content to account for both spheroid growth and population size (Gouws et al., 2021). From day 6 to day 12, there was some fluctuation in ATP per protein, after which the ATP per protein remained stable with small but consistent increases until day 22. This finding implied that the model was both metabolically stable and viable during this time. From day 24, the intracellular ATP per protein started to decrease and fluctuate, which could suggest a decrease in the viability of the spheroids (Kijanska and Kelm, 2016).

4.2.4 Extracellular adenylate content

Figure 10 (D) shows the extracellular AK per protein released from the cisplatin MDA-MB-231 spheroids per protein, shown as a function of time. AK release per protein increased between days 6 and 12, possibly due to stress and damage to the cells caused by handling the spheroids on day 6. In addition, this could result from the cells adapting from a 2D to a 3D environment. AK release then decreased to 14 and remained relatively stable until day 28, with minor changes. These results correlated with the stable ATP/protein values in the same period, suggesting the model was stable and viable with no significant cell death in this period.

4.2.5 Approximate glucose consumption

This parameter indicates cellular metabolic activity during spheroid growth (Gouws et al., 2021). An average of 21.4 mmol/L of glucose was found in the fresh growth media (n = 3). The overall approximate glucose intake per ClinoReactor™ was calculated by deducting the glucose content of the spent medium from the average glucose content of the fresh culture medium. As shown in Figure 10 (E), the glucose consumption per protein was calculated by normalizing it to the total protein content in each ClinoReactor™ by multiplying the number of spheroids by the protein content per

spheroid. This allowed for the presence of biomass to be compensated for. Each ClinoReactor™ received a new supply of growth medium on day 6 after the spheroids were sorted.

The glucose consumption per protein sharply increased until day 10 but decreased again towards day 12. From day 12 to day 28, the glucose consumption per protein remained relatively stable but still higher than day 6. The results show that throughout the 28 days of characterization, the spheroids were metabolically active, but the model did not consume large amounts of glucose. This correlates with slow growth and limited ATP production.

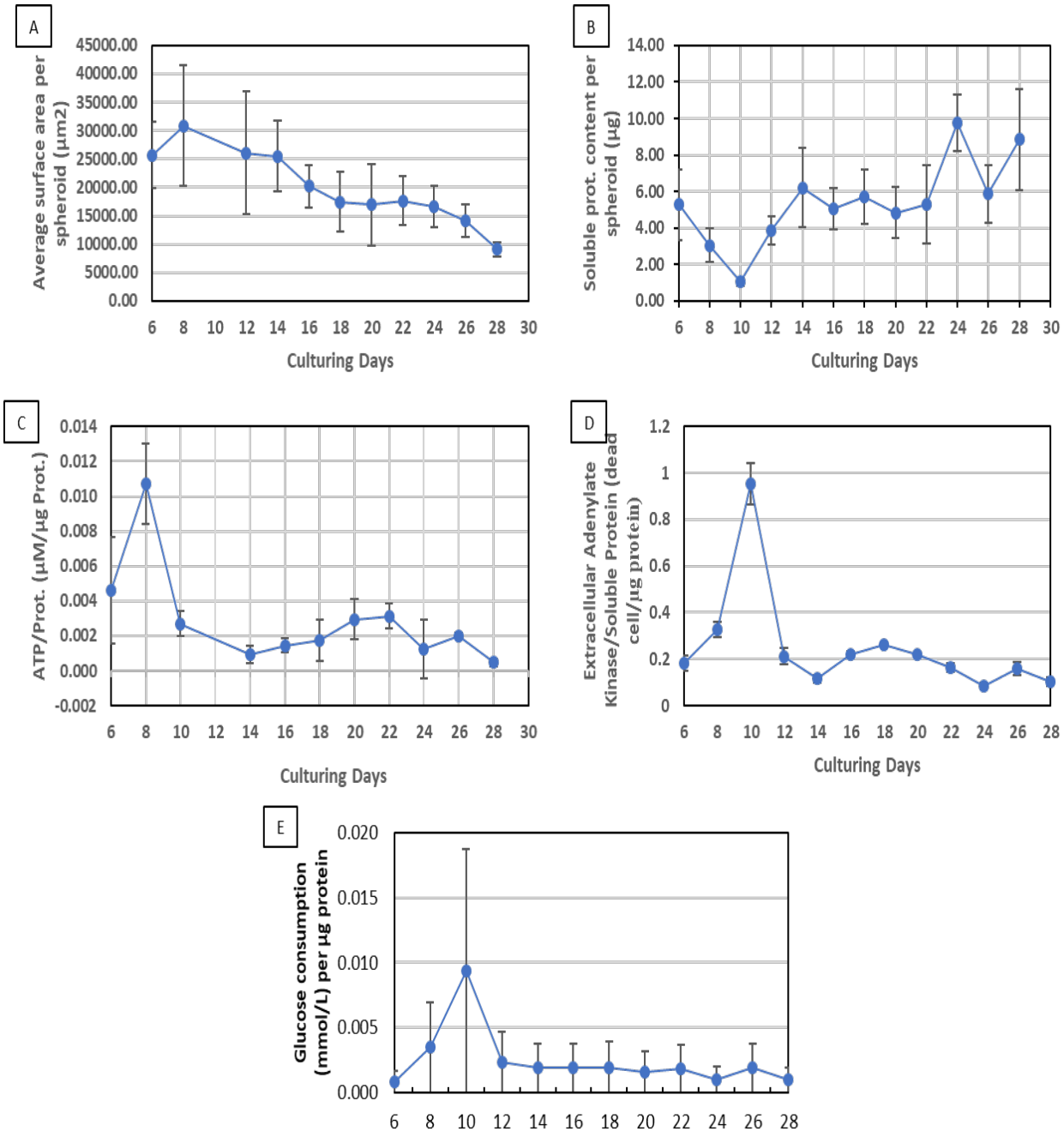

Figure 10. Characterization of the cisplatin-MDA-MB-231 spheroid model as a function of time in terms of (A) average planar surface area per spheroid (µm2), (B) soluble protein content per spheroid (µg), (C) intracellular adenosine triphosphate content per soluble protein content per spheroid (µg), (C) intracellular adenosine triphosphate content per soluble protein (µM/µg), (D) extracellular adenylate kinase release per µg protein and (e) approximate glucose consumption (mmol/L) per µg protein. Error bars = standard deviation

4.3 Qualification of the cisplatin-resistant MDA-MB-231 spheroid model reactivity to chemotherapeutic treatment

The cisplatin-resistant MDA-MB-231 spheroid model's reactivity to conventional chemotherapeutic treatments needed to be assessed in order for it to be deemed appropriate for anticancer therapy activity screening. Two common drugs, cisplatin and doxorubicin, were used as model drugs. These treatments were administered to the spheroid groups at the clinical doses for doxorubicin and cisplatin (60 mg/m^2 and 25 mg/m^2) used to treat TNBC patients, and a 2D IC_{50} dose (10.90 µM) for cisplatin for 96 h. Every data point was standardized in relation to the untreated control group. The treatment evaluation was conducted using the same spheroid initiation and maintenance protocols that were utilized to define the model.

4.3.1 Cisplatin clinical dose treatment

Soluble protein content: Measurements were made of each spheroid's soluble protein content during the 96-h treatment period with a cisplatin clinical dose (4.435×10^{-6} µg cisplatin/µg protein), as seen in Figure 11 (A). It was observed that the soluble protein content (µg) of the cisplatin clinical dose-treated spheroids decreased relative to the untreated control group in the first 24 h (0.39±0.3 µg), followed by a significant increase ($p=0.0099$) in protein content after 48 h (1.81±0.4 µg). It has been reported that cells can produce high amounts of protein in response to a toxic environment or chemical stimulus to regulate the tumour environment for adaptation and survival (Tilsed et al., 2022). Following this increase in protein, there was a notable reduction at 72 h (0.22±0.3 µg) and a further significant decrease ($p<0.0001$) at 96 h (0,19 µg) relative to the untreated control group.

Intracellular ATP/protein content: referring to Figure 11 (B), after an initial slight increase, at 48 h (0.38±0.3 µM/µg), a significant decrease ($p=0.0004$) was observed in the intracellular ATP/protein results. This was followed by a constant linear increase to 72 h (2.34±0.6 µM/µg) and 96 h (3.53±1.2 µM/µg), to elevated levels compared to the untreated group.

Approximate glucose consumption: the estimated quantities of glucose consumed by cells in each treatment group (mmol/L) were corrected to the amount of protein in the ClinoReactors™. The data was normalized to the untreated control group's approximate glucose consumed per µg protein. Following exposure, the cisplatin clinical dose-treated group showed normalized glucose consumption (1.12 mmol/L), similar to what was observed in the untreated control group after 24 h (1 mmol/L). A decrease in glucose consumed per µg protein was evident after 48 h of treatment (0.17 mmol/L), followed by a constant linear increase similar to that of the ATP/Prot levels in Figure 12 (B), with 1.72 mmol/L after 96 h of exposure.

Extracellular adenylate kinase content: the AK/protein released for the cisplatin clinical dose-treated group, as seen in Figure 11 (D), increased significantly ($p=0.0006$) after 24 h of treatment (4.53±0.5 dead cells/µg prot), followed by a decrease while remaining elevated relative to the untreated control. Another significant increase ($p<0.0001$) was observed after 72 h (6.82±2.9 dead cells/µg prot). A further decline of cell death per protein was noted at 96 h (4.52±1.7 dead cells/µg prot), but it was still significantly higher ($p<0.0001$) compared to the untreated control.

Planimetric measurement: the planimetry of the spheroids treated with the cisplatin clinical dose, as seen in Figure 11 (E), showed an initial increase in spheroid size during the first 24 h treatment. The spheroids then displayed a constant slow decrease in size throughout the 96 h treatment period, suggesting shrinkage or cell death, which correlates with the increased extracellular AK observed. However, the size did not decrease below that of the untreated control.

Photomicrograph: Figure 11 (Fa & Fc) illustrates the visual decrease in spheroid size observed in the treated group relative to the untreated control group for 96 h. The spheroids appear to be somewhat compact after 96 h of treatment.

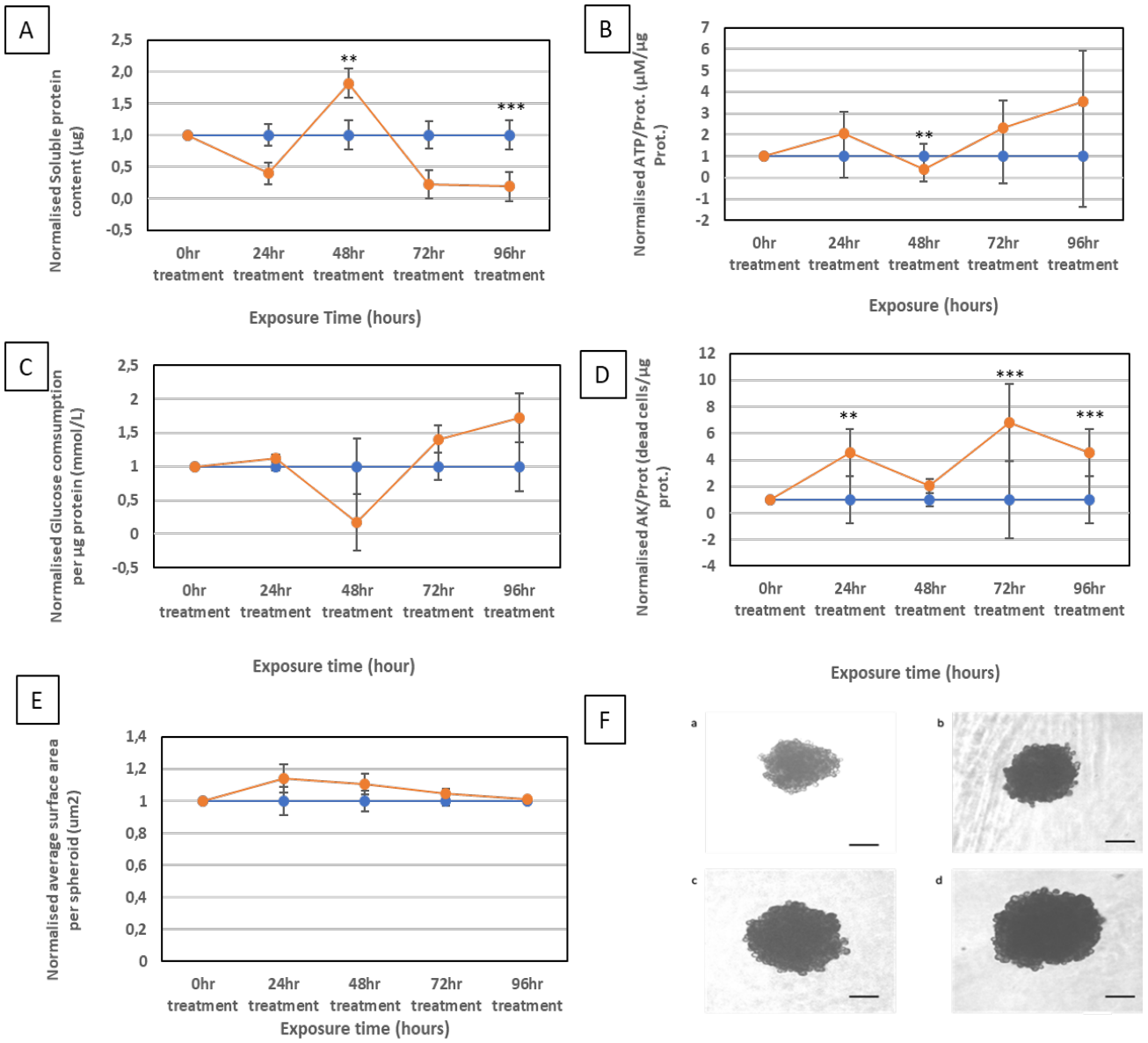

Figure 11. Evaluation of the cisplatin-resistant MDA-MB-231 spheroid model reactivity **following cisplatin clinical dose treatment** as a function of time, in terms of normalized (A) soluble protein content per spheroid (µg), (B) intracellular adenosine triphosphate content per soluble protein (µM/µg), (C) approximate glucose consumption (mmol/L) per µg protein, (D) extracellular adenylate kinase release per µg protein and (E) average planar surface area per spheroid (μm^2). The blue line represents the normalized untreated control group, and the orange line represents the cisplatin clinical dose-treated group normalized relative to the untreated control. (N=6, error bars = standard deviation; *= statistically significant, $p< 0.05$; **= statistically significant, $p<0.001$; ***= statistically highly significant, $p<0.0001$). (F) Photomicrographs of the (a) cisplatin clinical dose treatment group at 0 h of treatment, (b) untreated control group at 0 h, (c) cisplatin clinical dose treatment group after 96 h of treatment, and (d) untreated control group after 96 h (4x magnification; scale bar = 200 µm).

4.3.2 Doxorubicin clinical dose treatment

Soluble protein content: exposure to a doxorubicin clinical dose treatment (1,064 x 10^{-5} µg dox/µg protein), for 96 h, as seen in Figure 12 (A), resulted in a decrease in protein content after 24 h (0.46±0.2 µg) when compared to the untreated control group. This was followed by a significant increase ($p=0.0011$) after 48 h of treatment (2.10±0.5 µg). This may suggest higher protein production levels in the spheroids as a reactivity to the doxorubicin treatment. After 72 h (0.54±0.2 µg) treatment, the protein levels decreased to below that of the untreated control, and by 96 h (0.22±0.3 µg) of treatment, it was significantly ($p<0.0001$) decreased.

Intracellular ATP/protein content: The ATP/Prot levels, as seen in Figure 12 (B), decreased significantly ($p<0.0001$) after 48 h treatment to 0.14±0.4 µM/µg, followed by an increase to 1.12±0.06 µM/µg (72 h). There was a further significant rise ($p=0.0003$) to 3.45±1.4 µM/µg after 96 h exposure.

Approximate glucose consumption: The glucose consumed, Fig 12 (C), slightly decreased to 0.76 mmol/L at 24 h; this trend continued to 48 h (0.17 mmol/L) compared to the untreated control group (1.00 mmol/L). However, after 72 h, the glucose consumed increased again (0.85 mmol/L) and peaked at 96 h (3.67 mmol/L), a significant increase ($p<0.0001$) relative to the untreated control group.

Extracellular adenylate kinase content: the AK released per µg of protein, as seen in Figure 12 (D), indicated significant cell death after 24 h of treatment (3.63±1.3 dead cells/µg), and this continued to increase significantly with 2.76±0.8 dead cells/µg after 48 h ($p=0.0015$), 6.25±2.6 dead cells/µg at 72 h ($p<0.0001$), followed by a slight decrease to 96 h (5.14±2.0 dead cell/µg). This was, however, still significantly ($p<0.0001$) elevated relative to the untreated control.

Planimetric measurement: Considering the planimetry as seen in Figure 12 (E), a slight increase in the size of the spheroids was observed following 24 h of treatment (1,12 μm^2), followed by a steady decrease in size throughout the treatment period, albeit not

significantly so. In light of the increase in AK, this decrease in size was probably a result of cell death.

Photomicrogram: Figure 12 (Fa & Fc) illustrates the decrease in spheroid size observed as a result of treatment for 96 h when comparing them to the untreated control group for Figure 12 (Fb & Fd).

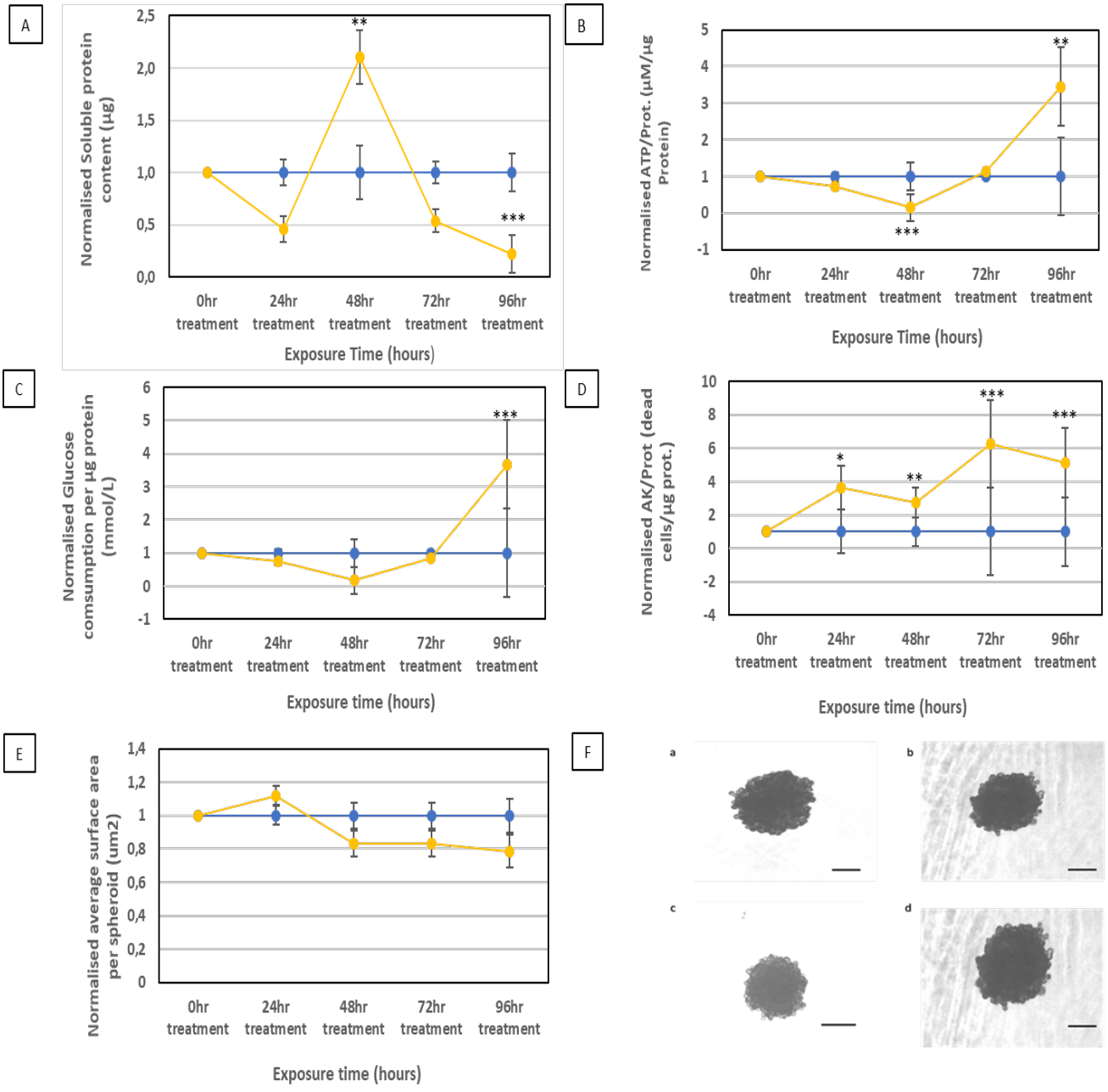

Figure 12. Evaluation of the cisplatin-resistant MDA-MB-231 spheroid model reactivity following **doxorubicin clinical dose treatment** as a function of time, in terms of normalized (A) soluble protein content per spheroid (µg), (B) intracellular adenosine triphosphate content per soluble protein (µM/µg), (C) approximate glucose consumption (mmol/L) per µg protein (D) extracellular adenylate kinase release per µg protein, and (E) average planar surface area per spheroid (μm^2). The blue line represents the normalized untreated control group, and the yellow line represents the doxorubicin clinical dose-treated group normalized relative to the untreated control. (N=6, error bars = standard deviation; *=

statistically significant, p< 0.05; **= statistically significant, p<0.001; ***= statistically highly significant, p<0.0001). (F) Photomicrographs of the (a) doxorubicin clinical dose treatment group at 0 h of treatment, (b) untreated control group at 0 h, (c) doxorubicin clinical dose treatment group after 96 h of treatment, and (d) untreated control group after 96 h (4x magnification; scale bar = 200 µm).

4.3.3 Cisplatin IC_{50} treatment

Soluble protein content: The soluble protein content, Figure 13 (A), had decreased significantly (p<0.0259) after 24 h (0.28±0.3 µg) of treatment (8.06 x 10^{-2} µg cisplatin/µg protein), followed by a significant increase (p=0.0030) by 48 h (2.04±0.5 µg). At 72 h, treatment levels decreased to levels similar to those after 24 h (0.30±0.3 µg), followed by a continuous significant decrease (p<0,0001) to 96 h (0.09±0.4 µg).

Intracellular ATP/protein content: An increase in the ATP/Prot levels were observed (Figure 13 (B)) following 24 h (2.21±0.6 µM/µg) of treatment, followed by a significant decrease (p=0.0002) of ATP/Prot production to 48 h (0.25±0.3 µM/µg). A linear increase in ATP/Prot levels followed, increasing above the untreated control group after 72 h (1.28±0.1 µM/µg) and at 96 h (2.51±0.7 µM/µg) of treatment.

Approximate glucose consumption: The estimated quantity of glucose consumed (Figure 13 (C)) increased significantly (p=0.0034) after 24 h (4.69 mmol/L) of treatment as the soluble protein values decreased compared to the untreated control group. This possibly indicates that the spheroids consumed more glucose to produce the energy required to overcome the effect of the treatment (Gouws et al., 2021). However, a decrease was observed after 48 h (0.04 mmol/L) relative to the untreated control. At 72 h (0.64 mmol/L) and 96 h (1.77 mmol/L), glucose levels increased linearly to levels slightly greater than the untreated control group, as though cells had recovered from the effects of the cisplatin IC_{50} treatment.

Extracellular adenylate kinase content: When considering cell death, Figure 13 (D), a significant increase (p<0.0001) relative to the untreated control was observed after 24 h (8.57±3.7 dead cell/µg) of treatment. This was followed by a decrease in AK released between 48 h (4.12±1.5 dead cell/µg) and 96 h (2.86±0.9 dead cell/µg) of treatment;

however, levels remained significantly greater ($p<0.0001$) compared to the untreated control group.

Planimetric measurements: According to the planimetric measurements, the spheroid size remained stable for the first 48 h of treatment, as indicated in Figure 13 (E), followed by a slight increase after 72 h of treatment; the spheroid size was then maintained until 96 h.

Photomicrogram: Figure 13 (F) shows that the treatment did not have a significant effect on the size and shape of the spheroids, although the spheroid integrity and shape appeared slightly less defined and compact.

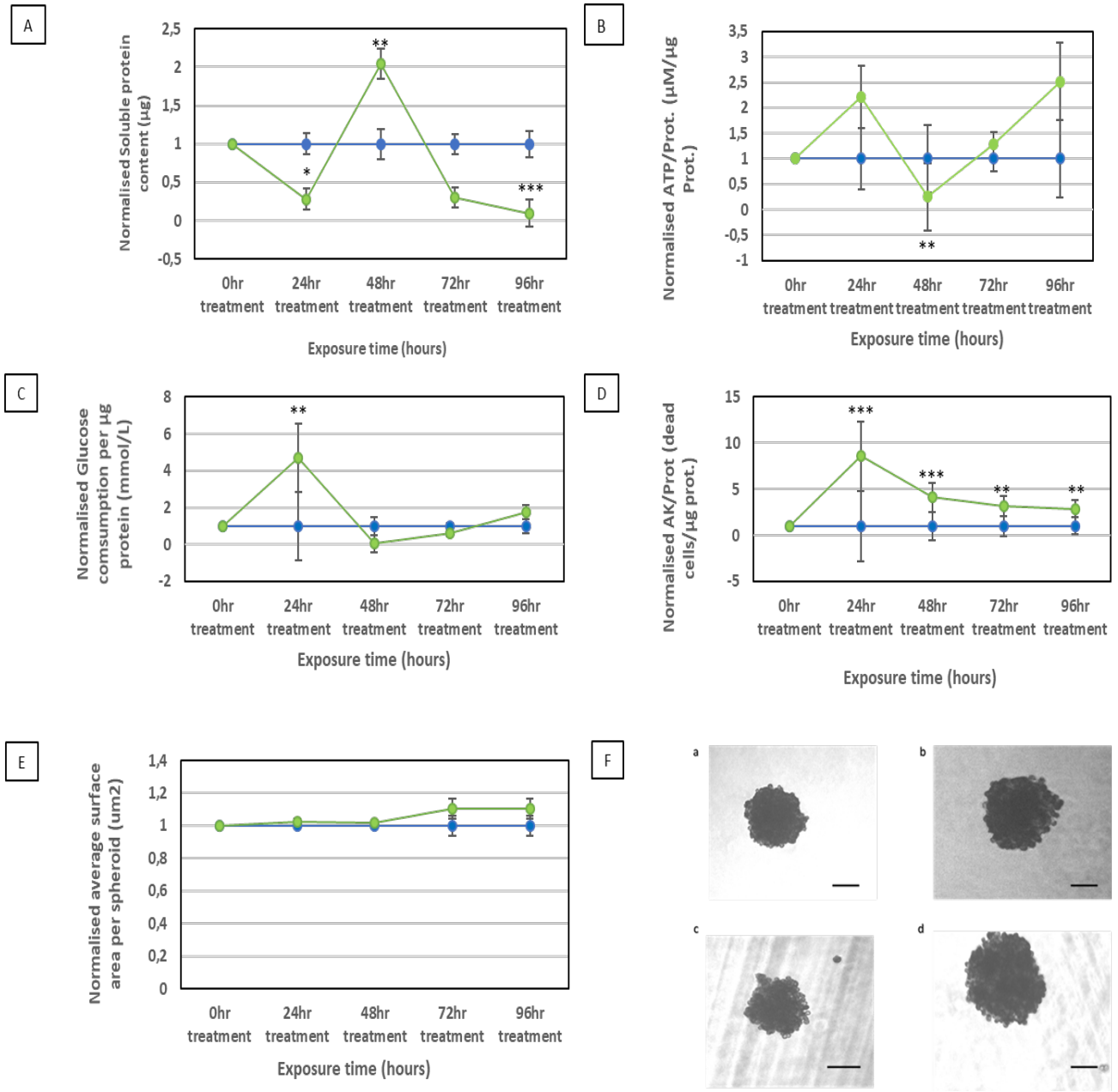

Figure 13. Evaluation of the cisplatin-resistant MDA-MB-231 spheroid model reactivity following **cisplatin IC_{50} treatment as a function** of time in terms of normalized (A) soluble protein content per spheroid (µg), (B) intracellular adenosine triphosphate content per spheroid (µg), (C) approximate glucose consumption (mmol/L) per µg protein (D) extracellular adenylate kinase release per µg protein, and (E) average planar surface area per spheroid (µm2). The blue line represents the normalized untreated control group, and the green line represents the cisplatin IC_{50} dose-treated group. (N=6, error bars = standard deviation; *= statistically significant, $p< 0.05$; **= statistically significant, $p<0.001$; ***= statistically highly significant, $p<0.0001$), (F) Photomicrographs of the (a) cisplatin IC_{50} treatment group at 0 h of treatment, (b) untreated control group at 0 h, (c) cisplatin IC_{50} treatment group after 96 h of treatment, and (d) untreated control group at 96 h (4x magnification; scale bar = 200 µm).

CHAPTER 5 – DISCUSSION

Traditional 2D cell culture models have been used extensively to assess cytotoxicity and are frequently employed in cancer research. However, this method fails to adequately replicate the *in vivo* system where the interaction between components of the TME, such as the extracellular environment, can significantly influence the drug response (Nowacka et al., 2022). Therefore, this study aimed to develop a novel cisplatin-resistant MDA-MB-231 spheroid model and evaluate the reactivity of the model to chemotherapeutic agents commonly used in treating TNBC. The model was developed using a scaffold-free CelVivo™ ClinoStar™ system that allows for the self-aggregation of single cells forming spheroids that closely represent *in vivo* solid tumours to address the shortcomings of conventional culture models.

Parameters such as intracellular ATP production, extracellular AK release, and approximate glucose consumption were employed to characterize the activity, growth, and viability of the cisplatin-resistant MBA-MB-231 spheroid model. During the experiment, these parameters were corrected per microgram of protein in each bioreactor to account for the alterations in the biomass, as spheroids both grew and were removed every sampling day. Due to the close relationship between intracellular ATP production and extracellular AK release, these two parameters are crucial in evaluating the health and growth of spheroids. ATP, the energy source of cells, is produced from metabolic reactions like glycolysis in the cytosol and oxidative phosphorylation in the mitochondria; levels of this compound enable us to measure cell viability, including growth, using bioluminescence (Ahmann et al., 1987). However, since the AK enzyme gets released into the extracellular region upon cell death, the extracellular AK assay aids in monitoring cellular health (Jacobs et al., 2013). Cancer cells undergo cell death by two processes. Apoptosis is energy-dependent programmed cell death by damaging DNA resulting from detected abnormal cells (Pfeffer and Singh, 2018). In necrosis, spontaneous cell death is mediated by low blood flow to the tissues of the cells and

exposure to toxic reagents that limit oxygenated blood to the rest of the cell, and is usually energy-independent (Liu and Jiao, 2019).

To confirm the reliability and effectiveness of the cisplatin-resistant MDA-MB-231 spheroid model for use during drug development and screening, the model's reactivity to treatment with two chemotherapeutic drugs (cisplatin and doxorubicin) was evaluated for a period of 96 h. During this period, treatment was replaced every 24 h while the same parameters employed for the model characterization were used to investigate the model's response to the relevant drugs. The treatment concentrations were selected as cisplatin (4.435×10^{-6}µg cisplatin/µg protein) and doxorubicin (1.064×10^{-5}µg dox/µg protein) clinical doses, derived from patient treatment doses for TNBC in clinical settings. Secondly, a cisplatin IC_{50} concentration (8.06×10^{-2} µg cisplatin/µg protein) determined from the MTT assay was included as an increased dose.

Characterization of the cisplatin-resistant MDA-MB-231 spheroid model

During the characterization of the model, the growth of the spheroids was evaluated through measurements such as spheroid surface area, soluble protein content, and visualization of the spheroids over time. The soluble content per spheroid as a function of time was evaluated for 28 days, and during this period, some fluctuation was observed (Figure 10 A) until day 14 in culture. This is normal and expected (van Niekerk et al., 2023) due to the handling during the sorting process, as well as the adaptation of the spheroid to a new environment. The cells in the spheroids need to adapt from the 2D environment to the 3D environment. However, the protein content per spheroid remained relatively stable from day 14 to day 22, suggesting stable cell viability in the cells, although no significant growth or death of spheroids was reported at this time. Instability in the protein content was again observed from day 24. The planimetric measurements did show some decrease in spheroid size over time, but this was a slow decrease that stabilized between days 16 and 24 in culture. Since no significant cell death was observed at this time, and visually, the spheroids appeared to compact, the decrease in size was most probably due to compacting and not loss of viability. Spheroid size did decrease faster from day 24. The images in Figure 10 (F-G) echoed the results, showing that the

spheroids started becoming fragile and less compact, and decreased drastically in size as they broke apart. Upon observation of the model and as reflected by the photomicrographs (Figure 9), the cisplatin-resistant MDA-MB-231 spheroids had a specific morphology and manner of growth and proliferation echoed by the peripheral cell layers. Finger-like projections of cells growing outward resulted in a rough edge of the spheroids. In a previous study (Huang et al., 2020), photomicrographs of MDA-MB-231 spheroids presented the same morphology and growth as the current spheroids. Previous studies suggest that EMT's role significantly impacts the spheroids' morphology with factors such as e-cadherin accumulation leading to inhibited formation of compact spheroids (Gunay et al., 2020). In this study we observed that spheroids reflected a loose morphology with no definite outline of the outer membrane that would instead enhance the spherical shape that is known to tumour cells. Commonly, TNBC is associated with the cellular program of EMT that confers drug resistance and metastasis (Huang et al., 2015). Thus, the resistance in the model in this study can be enhanced by the EMT properties exhibited by MDA-MB-231 cells.

In terms of spheroid viability during the model characterization, the levels of the ATP and AK also demonstrated the instability during the first days of model adaptation, but then remained relatively stable from day 12 to 22. This suggested a period of metabolic equilibrium where limited cell death occurred and no rapid growth or metabolic changes. The constant glucose consumption in this time period also supports this conclusion, as seen in Figure 10 E. From day 24, the energy production and growth of the spheroids were less stable, and then on day 28, ATP production and spheroid size decreased notably. This reflects the loss of integrity and viability of the cells in this model at this time point.

Following the characterization of the newly established cisplatin-resistant MDA-MB-231 spheroid model, the period identified as the optimal experimental window where the model reached metabolic equilibrium was determined to be between days 12 and 22 of culture. This is the ideal time in which crucial cell viability-related investigations should be performed to ensure consistent results and data.

Qualification of the cisplatin-resistant MDA-MB-231 spheroid model reactivity to chemotherapeutic treatments

To qualify the model's use for evaluation of potential treatments for drug resistant TNBC, the reactivity to chemotherapeutic drugs cisplatin and doxorubicin was evaluated at the doses mentioned above. The same spheroid growth and viability parameters used for characterizing the model were also investigated during the model qualification. This model was expected to react to the different treatment doses based on the cytotoxic effects of each model drug, the dose administered, and the spheroid models' sensitivity or resistance to the drugs.

Clinical cisplatin dose treatment

The clinical cisplatin treatment (4.435×10^{-6} µg cisplatin/µg protein) calculated using the clinical setting dose per protein content) was administered daily to the spheroids, and their reactivity was analyzed for a period of 96 h relative to an untreated control group (Figure 11). The results revealed the following changes in terms of spheroid growth. Although the spheroid size initially increased slightly, this increase was not maintained. Similarly, the soluble protein content had a significant increase after 48 h treatment but continued to then decrease significantly until 96 h treatment. Visually, the spheroid size, structure, and compactness did not appear to be influenced by the treatment.

Regarding model viability, both the ATP/prot and the extracellular AK levels followed the same pattern over time. Both initially increased relative to the untreated control, followed by a decrease at 48 h. However, both then increased relative to the untreated control group at 72 and 96 h. Specifically, the extracellular AK release indicated significant cell death at 24, 72, and 96 h, relative to the untreated control group. The estimated glucose consumed during this treatment relative to the untreated control also reflected the results seen for the ATP/Prot, whereby less glucose was consumed at 48 h, followed by increased glucose consumption at 72 and 96 h compared to the untreated control group. ATP production was maintained throughout the treatment period, suggesting the observed cell death was likely through apoptosis.

Overall, the clinical cisplatin treatment results suggest that the cisplatin-resistant MDA-MB-231 spheroids displayed reactivity to treatment with the substance it was purported

to be resistant against. This was evident from the significantly increased cell death observed relative to the untreated control. However, despite the increased AK release, the spheroids did not decrease significantly in size, did not lose structural integrity, and maintained metabolic activity.

IC_{50} cisplatin dose treatment

A higher dose cisplatin treatment (8,06 x 10^{-2} µg cisplatin/µg protein), based on the MTT assay, was administered to the established 3D model, and the reactivity was assessed (Figure 13).

In terms of spheroid growth, the higher cisplatin concentration increased the spheroid size as observed in terms of the planimetric measurements as well as the visual observations. The spheroid structure and compactness also did not appear to be influenced by the treatment. The soluble protein content had a significant increase relative to the untreated control after 48 h treatment, but then decreased significantly by 96 h treatment.

In terms of model viability, ATP/prot levels were elevated compared to the untreated control at 24 h. Although a significant decrease was noted at 48 h, the ATP/prot levels continuously increased to 96 h where it was elevated relative to the untreated control. Approximate glucose consumed followed the same trend as the ATP/prot, but although it was significantly elevated compared to the untreated control after 24 h exposure, by 96 h, the glucose consumption was only slightly increased relative to the untreated group. The AK release indicated continuous and significant cell death for the duration of the treatment, but was most pronounced after 24 h of treatment. ATP production was maintained, indicating that the observed cell death was most probably active and, therefore, apoptotic in nature.

Overall, the IC_{50} cisplatin treatment results suggest that the cisplatin-resistant MDA-MB-231 spheroids displayed reactivity to treatment with the higher concentration of the substance it was reported to be resistant against. This was concluded based on the significantly increased cell death observed relative to the untreated control. Once again, however, the spheroids did not lose structural integrity but maintained metabolic activity and slightly increased in size.

Clinical doxorubicin dose treatment

The effects of the clinical dose doxorubicin treatment (1,064 x 10^{-5} µg dox/µg protein) on the cisplatin-resistant MDA-MB-231 spheroid model was investigated for cross-reactivity. Based on the results (Figure 12), growth of the spheroids was impacted by the treatment as indicated by the decrease in planimetric measurements and visual observations. Although the soluble protein content was significantly elevated relative to the untreated control after 48 h exposure, it then decreased to levels significantly lower than the untreated control by 96 h treatment.

Viability also appeared to have been impacted, as the ATP/prot level significantly decreased relative to the untreated control group after 48 h. Glucose consumption also decreased compared to that of the untreated control group in the first 48 h. However, both were significantly elevated relative to the untreated control after 96 h exposure. The AK release graph also showed a significant and continuous increase in cell death throughout the experimental period relative to the untreated control group. Although ATP was almost depleted after 48 h exposure, suggesting that the cell death observed at that time point could have been a result of necrosis, ATP production then increased significantly which would suggest that the cell death was then apoptotic in nature.

These results suggest that the doxorubicin clinical dose treatment had the most significant effect on the viability of the spheroids.

Conclusion

Considering all the treatment groups and their effects on the established cisplatin-resistant MDA-MB-231 spheroid model, it can be concluded that the model showed reactivity to all the treatments, albeit to different extents.

Both cisplatin concentrations impacted the spheroids in terms of increased cell death, although the clinical dose showed continuously increased AK release while the higher dose had a higher initial measure of AK release which then continuously decreased during the treatment. Furthermore, the lower cisplatin concentration initially increased the spheroid size, but then the planimetric measurements returned to that of the untreated control. In contrast, the IC_{50} treatment had negligible impact on the spheroid size until

72 h exposure, whereafter, the spheroids then increased in size relative to the untreated control. Although viability appeared to have been impacted by both concentrations' cisplatin, neither seemed to have significant effects on viability since ATP production and glucose consumption was only significantly affected at 24 or 48 h exposure. Visually, the spheroids maintained a compact structure with minimal breakage throughout the treatment period, suggesting that the spheroids exhibited solid cell-cell adhesions.

The results suggest that the spheroids, in large part, were resistant to the cisplatin treatment despite the increased cell death observed. Furthermore, the model appeared to become even more resistant during exposure to the higher concentration of cisplatin as it experienced decreasing cell death and increased growth. This supports the use of the model for screening of treatments targeting resistant TNBC.

The doxorubicin treatment resulted in very similar cell death patterns as observed following the cisplatin clinical dose treatment. However, ATP production and glucose consumption were affected more significantly. The doxorubicin treatment also reduced spheroid size, which was not observed following cisplatin treatment. Anthracyclines (doxorubicin) are known to target cell proliferation of cancer cells (Wahba and El-Hadaad, 2015), supporting the relevance of the model developed for treatment screening.

CHAPTER 6 – CONCLUSION

Currently, TNBC remains a complex topic for researchers as it still has a poor prognosis and is still the most unmanageable breast cancer subtype. TNBC research can be improved by better modeling the TME to understand better the complexities associated with this disease. Thus, transitioning to a more suitable preclinical model, such as 3D spheroids that more realistically recapitulate the *in vivo* situation, is necessary.

This study aimed to develop a cisplatin-resistant MDA-MB-231 spheroid model using the CelVivo™ ClinoStar™ system, a clinostat-based rotating wall bioreactor methodology. Both a cisplatin-resistant MDA-MB-231 cell line and a 3D spheroid model were successfully developed, and the spheroid model was characterized in terms of growth and viability for 28 days. Furthermore, the model's reactivity and resilience were assessed by subjecting it to different doses of chemotherapeutic drugs (cisplatin and doxorubicin) for 96 h.

The cisplatin-resistant MDA-MB-231 model was viable until at least 26 days in culture, and an optimal experimental window where the model was metabolically stable was identified to be between days 12 and 22 in culture.

The results suggested moderate reactivity of the model to the clinical dose cisplatin ($4{,}435 \times 10^{-6}$ µg cisplatin/µg protein) treatment in terms of elevated cell death, but growth and viability did not appear significantly impacted. This supported the purported resistance of the model to cisplatin treatment. Furthermore, the cisplatin IC_{50} concentration (8.06×10^{-2} µg cisplatin/µg protein) resulted in immediate reactivity of the model and a significant increase in cell death, but the model appeared to gain increased resistance as treatment continued. This was evident from the decreasing cell death and increased spheroid growth.

The doxorubicin clinical dose (1.064×10^{-5}µg dox/µg protein) treatment had the most pronounced effect on the model and resulted in decreased spheroid size. It was apparent

that the model was not as resistant to the doxorubicin treatment as it was to the cisplatin treatment.

The response of TNBC MCF-7 cells to cisplatin in a perfused 3D model was compared with a standard 2D cell culture in a study conducted by Liu et al. (Liu et al., 2018). As per their findings, cells that were cultivated in 3D after forming spheroids exhibited greater resistance against cisplatin in comparison to cells that were cultured in 2D. Additionally, they observed higher amounts of reactive oxygen species, indicating a physiological shift and an environment similar to the TME *in vivo*.

Imamura et al. looked into the use of 3D culture models to screen for drug activity in model drugs (Imamura et al., 2015). They found that the drug response of the breast cancer cell lines (BT-474, BT-549, and T-47D) was superior to that of 2D cultured cells when it came to replicating the crucial elements of the tumour microenvironment *in vivo*, including the 3D culture's resistance to the drug. Consistent with these results, spheroids cultivated in this investigation also exhibited a range of tumour characteristics *in vivo*, including decreased proliferation, as shown by a reduction in spheroid size and increased drug resistance to cisplatin's cytotoxic effects.

A study by Ncube et al. demonstrated that the TNBC BT-20 spheroid model exhibited *in vivo* properties such as varying cell structures and intercellular solid connections, furthermore the model in this study showed increased resistance to doxorubicin when compared to traditional monolayer cultures, hence displaying a better potential in being utilised as an *in vitro* model that closely recapitulates the human physiological tumour environment to perform drug resistance research (Ncube et al., 2023).

Fontoura and colleagues investigated cell growth, gene expression and drug resistance in different TNBC 2D and 3D cell line cultures. In their finding’s cells grown in 3D model were able to aggregate and form spheroids, and they noted increased cell-cell contact when comparing spheroid to 2D cells. Additionally, they reported cells grown in 3D models displayed increased resistance to dacarbazine, and cisplatin. These results suggest that 2D systems may produce insufficient and inaccurate information as they fail to

produce a close resemblance of the human physiological environment (Fontoura et al., 2020).

By using 3D cell culture models, we can bridge the gap between *in vitro* and *in vivo* drug screening for resistance to existing chemotherapeutic drugs. Thus, the model evaluated in this study was qualified to be fit for purpose and can be employed to screen potential treatments in terms of anticancer properties, drug delivery, and response in preclinical studies. The cisplatin-resistant MDA-MB-231 spheroid model can also be utilized as a model for screening drug-targeting resistance.

To evaluate the model further, it would be advisable to treat the spheroids for 96 h, and then investigate recovery of the model following cessation, to gain a better understanding of the models' resistance to cisplatin. Furthermore, it would be of interest to evaluate the expression of ABC transporters associated with resistance of cisplatin to confirm further the extent of resistance of the cisplatin-resistant MDA-MB-231 spheroid model.

LIMITATIONS OF THE STUDY

Limitations included the prolonged sorting periods required to ensure spheroid size consistency, involving disruptive handling that increased the risk of cell clumping and breakage. Addressing these challenges could enhance the model's utility and reliability in future research efforts.

REFERENCES

ABAD, E., GRAIFER, D. & LYAKHOVICH, A. 2020. DNA damage response and resistance of cancer stem cells. *Cancer Lett,* 474**,** 106-117.

ACS 2014. American Cancer Society: Breast Cancer Facts and Figures 2013-2014.

ADAMS, F., ZIMMERMANN, C. M., LUCIANI, P. & MERKEL, O. M. 2023. Chapter 9 - Microfluidics for nanopharmaceutical and medical applications. *In:* PEROZZIELLO, G., KRÜHNE, U. & LUCIANI, P. (eds.) *Microfluidics for Cellular Applications.* Elsevier.

AHMANN, F. R., GAREWAL, H. S., SCHIFMAN, R., CELNIKER, A. & RODNEY, S. 1987. Intracellular adenosine triphosphate as a measure of human tumor cell viability and drug modulated growth. *In vitro cellular & developmental biology,* 23**,** 474-480.

AHMED, M. B., ISLAM, S. U., SONN, J. K. & LEE, Y. S. 2020. PRP4 Kinase Domain Loss Nullifies Drug Resistance and Epithelial-Mesenchymal Transition in Human Colorectal Carcinoma Cells. *Mol Cells,* 43**,** 662-670.

ALAOUNA, M., PENNY, C., HULL, R., MOLEFI, T., CHAUKE-MALINGA, N., KHANYILE, R., MAKGOKA, M., BIDA, M. & DLAMINI, Z. 2023. Overcoming the Challenges of Phytochemicals in Triple Negative Breast Cancer Therapy: The Path Forward. *Plants,* 12**,** 2350.

ALGHUWAINEM, A., ALSHAREEDA, A. T. & ALSOWAYAN, B. 2019a. Scaffold-Free 3-D Cell Sheet Technique Bridges the Gap between 2-D Cell Culture and Animal Models. *Int J Mol Sci,* 20.

ALGHUWAINEM, A., ALSHAREEDA, A. T. & ALSOWAYAN, B. 2019b. Scaffold-Free 3-D Cell Sheet Technique Bridges the Gap between 2-D Cell Culture and Animal Models. *International Journal of Molecular Sciences,* 20**,** 4926.

AMABLE, L. 2016. Cisplatin resistance and opportunities for precision medicine. *Pharmacological Research,* 106**,** 27-36.

AMJAD, M. T., CHIDHARLA, A. & KASI, A. 2024. Cancer Chemotherapy. *StatPearls.* Treasure Island (FL) ineligible companies. Disclosure: Anusha Chidharla declares no relevant financial relationships with ineligible companies. Disclosure: Anup Kasi declares no relevant financial relationships with ineligible companies.: StatPearls Publishing

Copyright © 2024, StatPearls Publishing LLC.

ANDERSEN, T., AUK-EMBLEM, P. & DORNISH, M. 2015. 3D Cell Culture in Alginate Hydrogels. *Microarrays,* 4**,** 133-161.

ATHANASIOU, K. A., ESWARAMOORTHY, R., HADIDI, P. & HU, J. C. 2013. Self-organization and the self-assembling process in tissue engineering. *Annual review of biomedical engineering,* 15**,** 115.

BAEK, D. W., PARK, J. Y., LEE, S. J. & CHAE, Y. S. 2020. Impressive effect of cisplatin monotherapy on a patient with heavily pretreated triple-negative breast cancer with poor performance. *Yeungnam Univ J Med,* 37**,** 230-235.

BAKER, B. M. & CHEN, C. S. 2012. Deconstructing the third dimension: how 3D culture microenvironments alter cellular cues. *J Cell Sci,* 125**,** 3015-24.

BARRILA, J., RADTKE, A. L., CRABBÉ, A., SARKER, S. F., HERBST-KRALOVETZ, M. M., OTT, C. M. & NICKERSON, C. A. 2010. Organotypic 3D cell culture models: using the rotating wall vessel to study host–pathogen interactions. *Nature Reviews Microbiology,* 8**,** 791-801.

BERG, W. A., SECHTIN, A. G., MARQUES, H. & ZHANG, Z. 2010. Cystic breast masses and the ACRIN 6666 experience. *Radiologic Clinics,* 48**,** 931-987.

BHARDWAJ, P., AU, C. C., BENITO-MARTIN, A., LADUMOR, H., OSHCHEPKOVA, S., MOGES, R. & BROWN, K. A. 2019. Estrogens and breast cancer: Mechanisms involved in obesity-related development, growth and progression. *J Steroid Biochem Mol Biol,* 189**,** 161-170.

BOICHUK, S., GALEMBIKOVA, A., SITENKOV, A., KHUSNUTDINOV, R., DUNAEV, P., VALEEVA, E. & USOLOVA, N. 2017. Establishment and characterization of a triple negative basal-like breast cancer cell line with multi-drug resistance. *Oncol Lett,* 14**,** 5039-5045.

BRESLIN, S. & O'DRISCOLL, L. 2013. Three-dimensional cell culture: the missing link in drug discovery. *Drug Discov Today,* 18**,** 240-9.

BROWN, A., KUMAR, S. & TCHOUNWOU, P. B. 2019. Cisplatin-Based Chemotherapy of Human Cancers. *J Cancer Sci Ther,* 11.

CASSIDY, J. W., BATRA, A. S., GREENWOOD, W. & BRUNA, A. 2016. Patient-derived tumour xenografts for breast cancer drug discovery. *Endocrine-related cancer,* 23**,** T259-T270.

CHEN, X. B., FAZEL ANVARI-YAZDI, A., DUAN, X., ZIMMERLING, A., GHARRAEI, R., SHARMA, N. K., SWEILEM, S. & NING, L. 2023. Biomaterials / bioinks and extrusion bioprinting. *Bioactive Materials,* 28**,** 511-536.

COSTA, E. C., MOREIRA, A. F., DE MELO-DIOGO, D., GASPAR, V. M., CARVALHO, M. P. & CORREIA, I. J. 2016. 3D tumor spheroids: an overview on the tools and techniques used for their analysis. *Biotechnol Adv,* 34**,** 1427-1441.

DASARI, S., NJIKI, S., MBEMI, A., YEDJOU, C. G. & TCHOUNWOU, P. B. 2022. Pharmacological Effects of Cisplatin Combination with Natural Products in Cancer Chemotherapy. *Int J Mol Sci,* 23.

DASS, S. A., TAN, K. L., SELVA RAJAN, R., MOKHTAR, N. F., MOHD ADZMI, E. R., WAN ABDUL RAHMAN, W. F., TENGKU DIN, T. A. D. A.-A. & BALAKRISHNAN, V. 2021. Triple negative breast cancer: a review of present and future diagnostic modalities. *Medicina,* 57**,** 62.

DERAKHSHAN, F. & REIS-FILHO, J. S. 2022. Pathogenesis of Triple-Negative Breast Cancer. *Annu Rev Pathol,* 17**,** 181-204.

DESANTIS, C. E., MA, J., GAUDET, M. M., NEWMAN, L. A., MILLER, K. D., GODING SAUER, A., JEMAL, A. & SIEGEL, R. L. 2019. Breast cancer statistics, 2019. *CA Cancer J Clin,* 69**,** 438-451.

DING, Y., LIU, W., YU, W., LU, S., LIU, M., KAPLAN, D. L. & WANG, X. 2018. Three-dimensional tissue culture model of human breast cancer for the evaluation of multidrug resistance. *Journal of tissue engineering and regenerative medicine,* 12**,** 1959-1971.

DLAMINI, Z., MOLEFI, T., KHANYILE, R., MKHABELE, M., DAMANE, B., KOKOUA, A., BIDA, M., SAINI, K. S., CHAUKE-MALINGA, N., LUVHENGO, T. E. & HULL, R. 2024. From Incidence to Intervention: A Comprehensive Look at Breast Cancer in South Africa. *Oncol Ther,* 12**,** 1-11.

DOGAN, B. E., LE-PETROSS, C. H., STAFFORD, J. R., ATKINSON, N. & WHITMAN, G. J. 2012. MRI-guided vacuum-assisted breast biopsy performed at 3 T with a 9-gauge needle: preliminary experience. *American Journal of Roentgenology,* 199**,** W651-W653.

DROST, J. & CLEVERS, H. 2018. Organoids in cancer research. *Nature Reviews Cancer,* 18**,** 407-418.

EDMONDSON, R., BROGLIE, J. J., ADCOCK, A. F. & YANG, L. 2014. Three-dimensional cell culture systems and their applications in drug discovery and cell-based biosensors. *Assay Drug Dev Technol,* 12**,** 207-18.

EIRO, N., GONZALEZ, L. O., FRAILE, M., CID, S., SCHNEIDER, J. & VIZOSO, F. J. 2019. Breast Cancer Tumor Stroma: Cellular Components, Phenotypic Heterogeneity, Intercellular Communication, Prognostic Implications and Therapeutic Opportunities. *Cancers (Basel),* 11.

ELMORE, S. 2007. Apoptosis: a review of programmed cell death. *Toxicol Pathol,* 35**,** 495-516.

EVE, L., FERVERS, B., LE ROMANCER, M. & ETIENNE-SELLOUM, N. 2020. Exposure to endocrine disrupting chemicals and risk of breast cancer. *International Journal of Molecular Sciences,* 21**,** 9139.

FAN, J., TO, K. K. W., CHEN, Z.-S. & FU, L. 2023. ABC transporters affects tumor immune microenvironment to regulate cancer immunotherapy and multidrug resistance. *Drug Resistance Updates,* 66**,** 100905.

FERLAY, J., COLOMBET, M., SOERJOMATARAM, I., PARKIN, D. M., PIÑEROS, M., ZNAOR, A. & BRAY, F. 2021. Cancer statistics for the year 2020: An overview. *Int J Cancer*.

FERREIRA, L. P., GASPAR, V. M. & MANO, J. F. 2018. Design of spherically structured 3D in vitro tumor models - Advances and prospects. *Acta Biomater,* 75**,** 11-34.

FIOLET, T., SROUR, B., SELLEM, L., KESSE-GUYOT, E., ALLÈS, B., MÉJEAN, C., DESCHASAUX, M., FASSIER, P., LATINO-MARTEL, P. & BESLAY, M. 2018. Consumption of ultra-processed foods and cancer risk: results from NutriNet-Santé prospective cohort. *bmj,* 360.

FONTOURA, J. C., VIEZZER, C., DOS SANTOS, F. G., LIGABUE, R. A., WEINLICH, R., PUGA, R. D., ANTONOW, D., SEVERINO, P. & BONORINO, C. 2020. Comparison of 2D and 3D cell culture models for cell growth, gene expression and drug resistance. *Materials Science and Engineering: C,* 107**,** 110264.

GALLUZZI, L., SENOVILLA, L., VITALE, I., MICHELS, J., MARTINS, I., KEPP, O., CASTEDO, M. & KROEMER, G. 2012a. Molecular mechanisms of cisplatin resistance. *Oncogene,* 31**,** 1869-83.

GALLUZZI, L., VITALE, I., ABRAMS, J. M., ALNEMRI, E. S., BAEHRECKE, E. H., BLAGOSKLONNY, M. V., DAWSON, T. M., DAWSON, V. L., EL-DEIRY, W. S., FULDA, S., GOTTLIEB, E., GREEN, D. R., HENGARTNER, M. O., KEPP, O., KNIGHT, R. A., KUMAR, S., LIPTON, S. A., LU, X., MADEO, F., MALORNI, W., MEHLEN, P., NUÑEZ, G., PETER, M. E., PIACENTINI, M., RUBINSZTEIN, D. C., SHI, Y., SIMON, H. U., VANDENABEELE, P., WHITE, E., YUAN, J., ZHIVOTOVSKY, B., MELINO, G. & KROEMER, G. 2012b. Molecular definitions of

cell death subroutines: recommendations of the Nomenclature Committee on Cell Death 2012. *Cell Death Differ,* 19**,** 107-20.

GALLUZZI, L., VITALE, I., MICHELS, J., BRENNER, C., SZABADKAI, G., HAREL-BELLAN, A., CASTEDO, M. & KROEMER, G. 2014. Systems biology of cisplatin resistance: past, present and future. *Cell Death Dis,* 5**,** e1257.

GARRIDO-CASTRO, A. C., LIN, N. U. & POLYAK, K. 2019. Insights into Molecular Classifications of Triple-Negative Breast Cancer: Improving Patient Selection for Treatment. *Cancer Discov,* 9**,** 176-198.

GERLINGER, M., ROWAN, A. J., HORSWELL, S., MATH, M., LARKIN, J., ENDESFELDER, D., GRONROOS, E., MARTINEZ, P., MATTHEWS, N., STEWART, A., TARPEY, P., VARELA, I., PHILLIMORE, B., BEGUM, S., MCDONALD, N. Q., BUTLER, A., JONES, D., RAINE, K., LATIMER, C., SANTOS, C. R., NOHADANI, M., EKLUND, A. C., SPENCER-DENE, B., CLARK, G., PICKERING, L., STAMP, G., GORE, M., SZALLASI, Z., DOWNWARD, J., FUTREAL, P. A. & SWANTON, C. 2012. Intratumor heterogeneity and branched evolution revealed by multiregion sequencing. *N Engl J Med,* 366**,** 883-892.

GINSBURG, O., BRAY, F., COLEMAN, M. P., VANDERPUYE, V., ENIU, A., KOTHA, S. R., SARKER, M., HUONG, T. T., ALLEMANI, C. & DVALADZE, A. 2017. The global burden of women's cancers: a grand challenge in global health. *The Lancet,* 389**,** 847-860.

GNANT, M., HARBECK, N. & THOMSSEN, C. 2017. St. Gallen/Vienna 2017: a brief summary of the consensus discussion about escalation and de-escalation of primary breast cancer treatment. *Breast Care,* 12**,** 101-106.

GÓMEZ-VIRGILIO, L., SILVA-LUCERO, M. D., FLORES-MORELOS, D. S., GALLARDO-NIETO, J., LOPEZ-TOLEDO, G., ABARCA-FERNANDEZ, A. M., ZACAPALA-GÓMEZ, A. E., LUNA-MUÑOZ, J., MONTIEL-SOSA, F., SOTO-ROJAS, L. O., PACHECO-HERRERO, M. & CARDENAS-AGUAYO, M. D. 2022. Autophagy: A Key Regulator of Homeostasis and Disease: An Overview of Molecular Mechanisms and Modulators. *Cells,* 11.

GONG, X., LIN, C., CHENG, J., SU, J., ZHAO, H., LIU, T., WEN, X. & ZHAO, P. 2015. Generation of Multicellular Tumor Spheroids with Microwell-Based Agarose Scaffolds for Drug Testing. *PLoS One,* 10**,** e0130348.

GOSLING, S., SCOTT, R., GREENWOOD, C., BOUZY, P., NALLALA, J., LYBURN, I. D., STONE, N. & ROGERS, K. 2019. Calcification microstructure reflects breast tissue microenvironment. *Journal of mammary gland biology and neoplasia,* 24**,** 333-342.

GOUWS, C., SMIT, T., WILLERS, C., SVITINA, H., CALITZ, C. & WRZESINSKI, K. 2021. Anticancer Potential of Sutherlandia frutescens and Xysmalobium undulatum in LS180 Colorectal Cancer Mini-Tumors. *Molecules,* 26**,** 605.

GUNAY, G., KIRIT, H. A., KAMATAR, A., BAGHDASARYAN, O., HAMSICI, S. & ACAR, H. 2020. The effects of size and shape of the ovarian cancer spheroids on the drug resistance and migration. *Gynecologic Oncology,* 159**,** 563-572.

GUNTI, S., HOKE, A. T. K., VU, K. P. & LONDON, N. R. 2021. Organoid and Spheroid Tumor Models: Techniques and Applications. *Cancers,* 13**,** 874.

GUTSCHNER, T. & DIEDERICHS, S. 2012. The hallmarks of cancer: a long non-coding RNA point of view. *RNA Biol,* 9**,** 703-19.

HABANJAR, O., DIAB-ASSAF, M., CALDEFIE-CHEZET, F. & DELORT, L. 2021. 3D cell culture systems: tumor application, advantages, and disadvantages. *International journal of molecular sciences,* 22**,** 12200.

HAN, S. J., KWON, S. & KIM, K. S. 2021. Challenges of applying multicellular tumor spheroids in preclinical phase. *Cancer Cell Int,* 21**,** 152.

HANAHAN, D. & WEINBERG, R. A. 2011. Hallmarks of cancer: the next generation. *Cell,* 144**,** 646-74.

HARBECK, N. & GNANT, M. 2017. Breast cancer. *Lancet,* 389**,** 1134-1150.

HAYCOCK, J. W. 2011. 3D cell culture: a review of current approaches and techniques. *Methods Mol Biol,* 695**,** 1-15.

HIDDING, J. T., BEURSKENS, C. H., VAN DER WEES, P. J., VAN LAARHOVEN, H. W. & NIJHUIS-VAN DER SANDEN, M. W. 2014. Treatment related impairments in arm and shoulder in patients with breast cancer: a systematic review. *PloS one,* 9**,** e96748.

HIEKEN, T. J. & BOUGHEY, J. C. 2016. Contralateral prophylactic mastectomy and its impact on quality of life. *Gland Surgery,* 5**,** 439.

HILL, C. & WANG, Y. 2020. The importance of epithelial-mesenchymal transition and autophagy in cancer drug resistance. *Cancer Drug Resist,* 3**,** 38-47.

HILL, D. A., PROSSNITZ, E. R., ROYCE, M. & NIBBE, A. 2019a. Temporal trends in breast cancer survival by race and ethnicity: A population-based cohort study. *PLoS One,* 14**,** e0224064.

HILL, D. P., HARPER, A., MALCOLM, J., MCANDREWS, M. S., MOCKUS, S. M., PATTERSON, S. E., REYNOLDS, T., BAKER, E. J., BULT, C. J., CHESLER, E. J. & BLAKE, J. A. 2019b. Cisplatin-resistant triple-negative breast cancer subtypes: multiple mechanisms of resistance. *BMC Cancer,* 19**,** 1039.

HIRSCHHAEUSER, F., MENNE, H., DITTFELD, C., WEST, J., MUELLER-KLIESER, W. & KUNZ-SCHUGHART, L. A. 2010. Multicellular tumor spheroids: an underestimated tool is catching up again. *J Biotechnol,* 148**,** 3-15.

HOARAU-VÉCHOT, J., RAFII, A., TOUBOUL, C. & PASQUIER, J. 2018. Halfway between 2D and Animal Models: Are 3D Cultures the Ideal Tool to Study Cancer-Microenvironment Interactions? *International Journal of Molecular Sciences,* 19**,** 181.

HOWES, B. H., WATSON, D. I., FOSH, B., YIP, J. M., KLEINIG, P. & DEAN, N. R. 2017. Magnetic resonance imaging versus 3-dimensional laser scanning for breast volume assessment after breast reconstruction. *Annals of plastic surgery,* 78**,** 455-459.

HUANG, J., LI, H. & REN, G. 2015. Epithelial-mesenchymal transition and drug resistance in breast cancer. *International journal of oncology,* 47**,** 840-848.

HUANG, Z., YU, P. & TANG, J. 2020. Characterization of Triple-Negative Breast Cancer MDA-MB-231 Cell Spheroid Model. *Onco Targets Ther,* 13**,** 5395-5405.

HUH, D., MATTHEWS, B. D., MAMMOTO, A., MONTOYA-ZAVALA, M., HSIN, H. Y. & INGBER, D. E. 2010. Reconstituting organ-level lung functions on a chip. *Science,* 328**,** 1662-1668.

HUSSAINI, H. 2017. Distinguishing Benign and Malignant Breast Mass using kinetic Curve of Dynamic contrast Enhanced MRI Scanning in Comparison with Histopathological Results. 14**,** 450-460.

IDRISOVA, K. F., SIMON, H. U. & GOMZIKOVA, M. O. 2022. Role of Patient-Derived Models of Cancer in Translational Oncology. *Cancers (Basel),* 15.

IMAMURA, Y., MUKOHARA, T., SHIMONO, Y., FUNAKOSHI, Y., CHAYAHARA, N., TOYODA, M., KIYOTA, N., TAKAO, S., KONO, S., NAKATSURA, T. & MINAMI, H. 2015. Comparison of 2D- and 3D-culture models as drug-testing platforms in breast cancer. *Oncol Rep,* 33**,** 1837-43.

ISMAIL, U. & KILLEEN, R. B. 2024. Taxane Toxicity. *StatPearls.* Treasure Island (FL) ineligible companies. Disclosure: Robert Killeen declares no relevant financial relationships with ineligible companies.: StatPearls Publishing

JACOBS, A. C., DIDONE, L., JOBSON, J., SOFIA, M. K., KRYSAN, D. & DUNMAN, P. M. 2013. Adenylate kinase release as a high-throughput-screening-compatible reporter of bacterial lysis for identification of antibacterial agents. *Antimicrobial agents and chemotherapy,* 57**,** 26-36.

JENSEN, C. & TENG, Y. 2020. Is it time to start transitioning from 2D to 3D cell culture? *Frontiers in molecular biosciences,* 7**,** 33.

JUBELIN, C., MUÑOZ-GARCIA, J., GRISCOM, L., COCHONNEAU, D., OLLIVIER, E., HEYMANN, M. F., VALLETTE, F. M., OLIVER, L. & HEYMANN, D. 2022. Three-dimensional in vitro culture models in oncology research. *Cell Biosci,* 12**,** 155.

KASSAM, F., ENRIGHT, K., DENT, R., DRANITSARIS, G., MYERS, J., FLYNN, C., FRALICK, M., KUMAR, R. & CLEMONS, M. 2009. Survival outcomes for patients with metastatic triple-negative breast cancer: implications for clinical practice and trial design. *Clin Breast Cancer,* 9**,** 29-33.

KENNY, P. A., LEE, G. Y., MYERS, C. A., NEVE, R. M., SEMEIKS, J. R., SPELLMAN, P. T., LORENZ, K., LEE, E. H., BARCELLOS-HOFF, M. H., PETERSEN, O. W., GRAY, J. W. & BISSELL, M. J. 2007. The morphologies of breast cancer cell lines in three-dimensional assays correlate with their profiles of gene expression. *Mol Oncol,* 1**,** 84-96.

KIJANSKA, M. A. & KELM, J. M. In vitro 3D Spheroids and Microtissues: ATP-based Cell Viability and Toxicity Assays. 2016.

KIM, D. H., XING, T., YANG, Z., DUDEK, R., LU, Q. & CHEN, Y. H. 2017. Epithelial Mesenchymal Transition in Embryonic Development, Tissue Repair and Cancer: A Comprehensive Overview. *J Clin Med,* 7.

KROEMER, G., GALLUZZI, L., VANDENABEELE, P., ABRAMS, J., ALNEMRI, E. S., BAEHRECKE, E., BLAGOSKLONNY, M., EL-DEIRY, W., GOLSTEIN, P. & GREEN, D. 2009. Classification of cell death: recommendations of the Nomenclature Committee on Cell Death 2009. *Cell death & differentiation,* 16**,** 3-11.

KUCZYNSKI, E. A., VERMEULEN, P. B., PEZZELLA, F., KERBEL, R. S. & REYNOLDS, A. R. 2019. Vessel co-option in cancer. *Nat Rev Clin Oncol,* 16**,** 469-493.

KUMMEROW, K. L., DU, L., PENSON, D. F., SHYR, Y. & HOOKS, M. A. 2015. Nationwide trends in mastectomy for early-stage breast cancer. *JAMA surgery,* 150**,** 9-16.

LANGHANS, S. A. 2018. Three-dimensional in vitro cell culture models in drug discovery and drug repositioning. *Frontiers in pharmacology,* 9**,** 6.

LESO, V., ERCOLANO, M. L., CIOFFI, D. L. & IAVICOLI, I. 2019. Occupational chemical exposure and breast cancer risk according to hormone receptor status: a systematic review. *Cancers,* 11**,** 1882.

LICATA, J. P., SCHWAB, K. H., HAR-EL, Y.-E., GERSTENHABER, J. A. & LELKES, P. I. 2023. Bioreactor Technologies for Enhanced Organoid Culture. *International Journal of Molecular Sciences,* 24**,** 11427.

LIU, G.-R., ZHANG, G., JIANG, F.-J., DING, X., SUN, Y., SUN, J. & MA, E. 2013. Nanostructured high-strength molybdenum alloys with unprecedented tensile ductility. *Nature materials,* 12**,** 344-350.

LIU, Q., ZHANG, Z., LIU, Y., CUI, Z., ZHANG, T., LI, Z. & MA, W. 2018. Cancer cells growing on perfused 3D collagen model produced higher reactive oxygen species level and were more resistant to cisplatin compared to the 2D model. *J Appl Biomater Funct Mater,* 16**,** 144-150.

LIU, X., INDA, M. E., LAI, Y., LU, T. K. & ZHAO, X. 2022. Engineered living hydrogels. *Advanced Materials,* 34**,** 2201326.

LIU, Z. G. & JIAO, D. 2019. Necroptosis, tumor necrosis and tumorigenesis. *Cell Stress,* 4**,** 1-8.

LOVELACE, D. L., MCDANIEL, L. R. & GOLDEN, D. 2019. Long-term effects of breast cancer surgery, treatment, and survivor care. *Journal of midwifery & women's health,* 64**,** 713-724.

LUGONES, Y., LOREN, P. & SALAZAR, L. A. 2022. Cisplatin Resistance: Genetic and Epigenetic Factors Involved. *Biomolecules,* 12.

ŁUKASIEWICZ, S., CZECZELEWSKI, M., FORMA, A., BAJ, J., SITARZ, R. & STANISŁAWEK, A. 2021. Breast Cancer—Epidemiology, Risk Factors, Classification, Prognostic Markers, and Current Treatment Strategies—An Updated Review. *Cancers,* 13**,** 4287.

MAMTANI, A. & MORROW, M. 2017. Why are there so many mastectomies in the United States? *Annual review of medicine,* 68**,** 229-241.

MANI, S. A., GUO, W., LIAO, M. J., EATON, E. N., AYYANAN, A., ZHOU, A. Y., BROOKS, M., REINHARD, F., ZHANG, C. C., SHIPITSIN, M., CAMPBELL, L. L., POLYAK, K., BRISKEN, C., YANG, J. & WEINBERG, R. A. 2008. The epithelial-mesenchymal transition generates cells with properties of stem cells. *Cell,* 133**,** 704-15.

MCDERMOTT, M., EUSTACE, A., BUSSCHOTS, S., BREEN, L., CLYNES, M., O'DONOVAN, N. & STORDAL, B. 2014a. In vitro Development of Chemotherapy and Targeted Therapy Drug-Resistant Cancer Cell Lines: A Practical Guide with Case Studies. *Frontiers in Oncology,* 4.

MCDERMOTT, M., EUSTACE, A., BUSSCHOTS, S., BREEN, L., CLYNES, M., O'DONOVAN, N. & STORDAL, B. 2014b. In vitro Development of Chemotherapy and Targeted Therapy Drug-Resistant Cancer Cell Lines: A Practical Guide with Case Studies. *Frontiers in Oncology,* 4.

MEHTA, G., HSIAO, A. Y., INGRAM, M., LUKER, G. D. & TAKAYAMA, S. 2012. Opportunities and challenges for use of tumor spheroids as models to test drug delivery and efficacy. *Journal of controlled release,* 164**,** 192-204.

MIYAZAKI, T., MIYAUCHI, S., MATSUZAKA, S., YAMAGISHI, C. & KOBAYASHI, K. 2010. Formation of proteoglycan and collagen-rich scaffold-free stiff cartilaginous tissue using two-step culture methods with combinations of growth factors. *Tissue Engineering Part A,* 16**,** 1575-1584.

MOHANTY, S. S. & MOHANTY, P. K. 2021. Obesity as potential breast cancer risk factor for postmenopausal women. *Genes Dis,* 8**,** 117-123.

MUGURUMA, M., TERAOKA, S., MIYAHARA, K., UEDA, A., ASAOKA, M., OKAZAKI, M., KAWATE, T., KURODA, M., MIYAGI, Y. & ISHIKAWA, T. 2020. Differences in drug sensitivity between two-dimensional and three-dimensional culture systems in triple-negative breast cancer cell lines. *Biochemical and Biophysical Research Communications,* 533**,** 268-274.

NAIR, A. B. & JACOB, S. 2016. A simple practice guide for dose conversion between animals and human. *J Basic Clin Pharm,* 7**,** 27-31.

NARDIN, S., MORA, E., VARUGHESE, F. M., D'AVANZO, F., VACHANARAM, A. R., ROSSI, V., SAGGIA, C., RUBINELLI, S. & GENNARI, A. 2020. Breast Cancer Survivorship, Quality of Life, and Late Toxicities. *Front Oncol,* 10**,** 864.

NAVARRO, C., ORTEGA, Á., SANTELIZ, R., GARRIDO, B., CHACÍN, M., GALBAN, N., VERA, I., DE SANCTIS, J. B. & BERMÚDEZ, V. 2022. Metabolic Reprogramming in Cancer Cells: Emerging Molecular Mechanisms and Novel Therapeutic Approaches. *Pharmaceutics,* 14.

NCUBE, K. N., JURGENS, T., STEENKAMP, V., CROMARTY, A. D., VAN DEN BOUT, I. & CORDIER, W. 2023. Comparative Evaluation of the Cytotoxicity of Doxorubicin in BT-20 Triple-Negative Breast Carcinoma Monolayer and Spheroid Cultures. *Biomedicines,* 11**,** 1484.

NEWMAN, L. A. & KALJEE, L. M. 2017. Health Disparities and Triple-Negative Breast Cancer in African American Women: A Review. *JAMA Surg,* 152**,** 485-493.

NGA, N. T. H., NGOC, T. T. B., TRINH, N. T. M., THUOC, T. L. & THAO, D. T. P. 2020. Optimization and application of MTT assay in determining density of suspension cells. *Anal Biochem,* 610**,** 113937.

NIKOLOVA, M. P. & CHAVALI, M. S. 2019. Recent advances in biomaterials for 3D scaffolds: A review. *Bioactive materials,* 4**,** 271-292.

NINDREA, R. D., ARYANDONO, T. & LAZUARDI, L. 2017. Breast cancer risk from modifiable and non-modifiable risk factors among women in Southeast Asia: a meta-analysis. *Asian Pacific journal of cancer prevention: APJCP,* 18**,** 3201.

NOLAN, J. C., FRAWLEY, T., TIGHE, J., SOH, H., CURTIN, C. & PISKAREVA, O. 2020. Preclinical models for neuroblastoma: Advances and challenges. *Cancer Lett,* 474**,** 53-62.

NOWACKA, M., GINTER-MATUSZEWSKA, B., ŚWIERCZEWSKA, M., STERZYŃSKA, K., NOWICKI, M. & JANUCHOWSKI, R. 2022. Effect of ALDH1A1 Gene Knockout on Drug Resistance in Paclitaxel and Topotecan Resistant Human Ovarian Cancer Cell Lines in 2D and 3D Model. *Int J Mol Sci,* 23.

NUNES, A. S., BARROS, A. S., COSTA, E. C., MOREIRA, A. F. & CORREIA, I. J. 2019. 3D tumor spheroids as in vitro models to mimic in vivo human solid tumors resistance to therapeutic drugs. *Biotechnol Bioeng,* 116**,** 206-226.

OAKMAN, C., VIALE, G. & DI LEO, A. 2010. Management of triple negative breast cancer. *The Breast,* 19**,** 312-321.

OVSIANIKOV, A., KHADEMHOSSEINI, A. & MIRONOV, V. 2018. The synergy of scaffold-based and scaffold-free tissue engineering strategies. *Trends in biotechnology,* 36**,** 348-357.

PARK, M., KIM, D., KO, S., KIM, A., MO, K. & YOON, H. 2022. Breast Cancer Metastasis: Mechanisms and Therapeutic Implications. *International Journal of Molecular Sciences,* 23**,** 6806.

PEART, O. 2015. Breast intervention and breast cancer treatment options. *Radiologic technology,* 86**,** 535M-558M.

PENAULT-LLORCA, F. & VIALE, G. 2012. Pathological and molecular diagnosis of triple-negative breast cancer: a clinical perspective. *Annals of oncology,* 23**,** vi19-vi22.

PETRELLI, F., BARNI, S., BREGNI, G., DE BRAUD, F. & DI COSIMO, S. 2016. Platinum salts in advanced breast cancer: a systematic review and meta-analysis of randomized clinical trials. *Breast Cancer Res Treat,* 160**,** 425-437.

PFEFFER, C. M. & SINGH, A. T. K. 2018. Apoptosis: A Target for Anticancer Therapy. *Int J Mol Sci,* 19.

QUAIL, D. F., BOWMAN, R. L., AKKARI, L., QUICK, M. L., SCHUHMACHER, A. J., HUSE, J. T., HOLLAND, E. C., SUTTON, J. C. & JOYCE, J. A. 2016. The tumor microenvironment underlies acquired resistance to CSF-1R inhibition in gliomas. *Science,* 352**,** aad3018.

RABIK, C. A., MARYON, E. B., KASZA, K., SHAFER, J. T., BARTNIK, C. M. & DOLAN, M. E. 2009. Role of copper transporters in resistance to platinating agents. *Cancer Chemother Pharmacol,* 64**,** 133-42.

RANASINGHE, R., MATHAI, M. L. & ZULLI, A. 2022. Cisplatin for cancer therapy and overcoming chemoresistance. *Heliyon,* 8**,** e10608.

REHMAN, S. 2018. An Overview of Cancer Treatment Modalities.

RODGERS, K. M., UDESKY, J. O., RUDEL, R. A. & BRODY, J. G. 2018. Environmental chemicals and breast cancer: An updated review of epidemiological literature informed by biological mechanisms. *Environmental research,* 160**,** 152-182.

RYU, N.-E., LEE, S.-H. & PARK, H. 2019. Spheroid culture system methods and applications for mesenchymal stem cells. *Cells,* 8**,** 1620.

SANT, S. & JOHNSTON, P. A. 2017. The production of 3D tumor spheroids for cancer drug discovery. *Drug Discovery Today: Technologies,* 23**,** 27-36.

SAXENA, M., STEPHENS, M. A., PATHAK, H. & RANGARAJAN, A. 2011. Transcription factors that mediate epithelial-mesenchymal transition lead to multidrug resistance by upregulating ABC transporters. *Cell Death Dis,* 2**,** e179.

SEYFRIED, T. N. & HUYSENTRUYT, L. C. 2013. On the origin of cancer metastasis. *Critical reviews in oncogenesis,* 18**,** 43-73.

SHARMA, A., BOISE, L. H. & SHANMUGAM, M. 2019. Cancer Metabolism and the Evasion of Apoptotic Cell Death. *Cancers,* 11**,** 1144.
SHIOVITZ, S. & KORDE, L. A. 2015. Genetics of breast cancer: a topic in evolution. *Annals of Oncology,* 26**,** 1291-1299.
SIMONS, B. & BRAYTON, C. 2017. Challenges and limitations of mouse xenograft models of cancer. *Patient Derived Tumor Xenograft Models.* Elsevier.
SINGH, A. & SETTLEMAN, J. 2010. EMT, cancer stem cells and drug resistance: an emerging axis of evil in the war on cancer. *Oncogene,* 29**,** 4741-51.
SMIT, T., CALITZ, C., WILLERS, C., SVITINA, H., HAMMAN, J., FEY, S. J., GOUWS, C. & WRZESINSKI, K. 2020. Characterization of an Alginate Encapsulated LS180 Spheroid Model for Anti-colorectal Cancer Compound Screening. *ACS Medicinal Chemistry Letters,* 11**,** 1014-1021.
SMITH, M. T., GUYTON, K. Z., KLEINSTREUER, N., BORREL, A., CARDENAS, A., CHIU, W. A., FELSHER, D. W., GIBBONS, C. F., GOODSON, W. H., 3RD, HOUCK, K. A., KANE, A. B., LA MERRILL, M. A., LEBREC, H., LOWE, L., MCHALE, C. M., MINOCHERHOMJI, S., RIESWIJK, L., SANDY, M. S., SONE, H., WANG, A., ZHANG, L., ZEISE, L. & FIELDEN, M. 2020. The Key Characteristics of Carcinogens: Relationship to the Hallmarks of Cancer, Relevant Biomarkers, and Assays to Measure Them. *Cancer Epidemiol Biomarkers Prev,* 29**,** 1887-1903.
TALMADGE, J. E. & FIDLER, I. J. 2010. AACR centennial series: the biology of cancer metastasis: historical perspective. *Cancer Res,* 70**,** 5649-69.
TIAN, H., LYU, Y., YANG, Y.-G. & HU, Z. 2020. Humanized rodent models for cancer research. *Frontiers in Oncology,* 10**,** 1696.
TILSED, C. M., FISHER, S. A., NOWAK, A. K., LAKE, R. A. & LESTERHUIS, W. J. 2022. Cancer chemotherapy: insights into cellular and tumor microenvironmental mechanisms of action. *Front Oncol,* 12**,** 960317.
TOSCA, E. M., RONCHI, D., FACCIOLO, D. & MAGNI, P. 2023. Replacement, Reduction, and Refinement of Animal Experiments in Anticancer Drug Development: The Contribution of 3D In Vitro Cancer Models in the Drug Efficacy Assessment. *Biomedicines,* 11**,** 1058.
TRUJILLO-DE SANTIAGO, G., FLORES-GARZA, B. G., TAVARES-NEGRETE, J. A., LARA-MAYORGA, I. M., GONZÁLEZ-GAMBOA, I., ZHANG, Y. S., ROJAS-MARTÍNEZ, A., ORTIZ-LÓPEZ, R. & ÁLVAREZ, M. M. 2019. The tumor-on-chip: Recent advances in the development of microfluidic systems to recapitulate the physiology of solid tumors. *Materials,* 12**,** 2945.
TUVESON, D. & CLEVERS, H. 2019. Cancer modeling meets human organoid technology. *Science,* 364**,** 952-955.
UNNIKRISHNAN, K., THOMAS, L. V. & RAM KUMAR, R. M. 2021. Advancement of Scaffold-Based 3D Cellular Models in Cancer Tissue Engineering: An Update. *Front Oncol,* 11**,** 733652.
VAN NIEKERK, A., WRZESINSKI, K., STEYN, D. & GOUWS, C. 2023. A Novel NCI-H69AR Drug-Resistant Small-Cell Lung Cancer Mini-Tumor Model for Anti-Cancer Treatment Screening. *Cells,* 12.
VAN RIJT, A., STEFANEK, E. & VALENTE, K. 2023. Preclinical Testing Techniques: Paving the Way for New Oncology Screening Approaches. *Cancers,* 15**,** 4466.
VANDERMIES, M. & FICKERS, P. 2019. Bioreactor-Scale Strategies for the Production of Recombinant Protein in the Yeast Yarrowia lipolytica. *Microorganisms,* 7**,** 40.
WAHBA, H. A. & EL-HADAAD, H. A. 2015. Current approaches in treatment of triple-negative breast cancer. *Cancer biology & medicine,* 12**,** 106.
WALRATH, J. C., HAWES, J. J., VAN DYKE, T. & REILLY, K. M. 2010. Genetically engineered mouse models in cancer research. *Adv Cancer Res,* 106**,** 113-64.
WANG, X., ZHANG, H. & CHEN, X. 2019. Drug resistance and combating drug resistance in cancer. *Cancer Drug Resist,* 2**,** 141-160.
WANGPAICHITR, M., THEODOROPOULOS, G., NGUYEN, D. J. M., WU, C., SPECTOR, S. A., FEUN, L. G. & SAVARAJ, N. 2021. Cisplatin Resistance and Redox-Metabolic Vulnerability: A Second Alteration. *Int J Mol Sci,* 22.
WENGERT, G. J., SCHMUTZER, M., BICKEL, H., SORA, M. C., POLANEC, S. H., WEBER, M. & SCHUELLER-WEIDEKAMM, C. 2019. Reliability of high-resolution ultrasound and magnetic resonance arthrography of the shoulder in patients with sports-related shoulder injuries. *PLoS One,* 14**,** e0222783.
WONG, C. H., SIAH, K. W. & LO, A. W. 2019. Estimation of clinical trial success rates and related parameters. *Biostatistics,* 20**,** 273-286.

WRZESINSKI, K. & FEY, S. J. 2013. After trypsinisation, 3D spheroids of C3A hepatocytes need 18 days to re-establish similar levels of key physiological functions to those seen in the liver. *Toxicology research,* 2**,** 123-135.

WRZESINSKI, K. & FEY, S. J. 2015. From 2D to 3D--a New Dimension for Modelling the Effect of Natural Products on Human Tissue. *Curr Pharm Des,* 21**,** 5605-16.

WRZESINSKI, K. & FEY, S. J. 2018. Metabolic Reprogramming and the Recovery of Physiological Functionality in 3D Cultures in Micro-Bioreactors. *Bioengineering (Basel),* 5.

WRZESINSKI, K. & J FEY, S. 2015. From 2D to 3D-a new dimension for modelling the effect of natural products on human tissue. *Current pharmaceutical design,* 21**,** 5605-5616.

ZHANG, Z. H., JHAVERI, D. J., MARSHALL, V. M., BAUER, D. C., EDSON, J., NARAYANAN, R. K., ROBINSON, G. J., LUNDBERG, A. E., BARTLETT, P. F., WRAY, N. R. & ZHAO, Q. Y. 2014. A comparative study of techniques for differential expression analysis on RNA-Seq data. *PLoS One,* 9**,** e103207.

ZHOU, Z., QUTAISH, M., HAN, Z., SCHUR, R. M., LIU, Y., WILSON, D. L. & LU, Z.-R. 2015. MRI detection of breast cancer micrometastases with a fibronectin-targeting contrast agent. *Nature communications,* 6**,** 7984.

ZHU, Z., DU, S., DU, Y., REN, J., YING, G. & YAN, Z. 2018. Glutathione reductase mediates drug resistance in glioblastoma cells by regulating redox homeostasis. *J Neurochem,* 144**,** 93-104.

APPENDICES

Appendix A: Ethics approval letter

UNIVERSITY OF THE FREE STATE
UNIVERSITEIT VAN DIE VRYSTAAT
YUNIVESITHI YA FREISTATA

UFS·UV
RESEARCH DEVELOPMENT
NAVORSINGSONTWIKKELING

Environment & Biosafety Research Ethics Committee

09-Feb-2023

Dear **Ongeziwe Ngalonkulu**

Project Title: **Establishing a cisplatin-resistant triple negative breast cancer spheroid model**

Department: **Pharmacology Department (Bloemfontein Campus)**

APPLICATION APPROVED

This letter confirms that this research proposal was given ethical clearance by the Environment & Biosafety Research Ethics Committee of the University of the Free State.

Your ethical clearance number, to be used in all correspondence is: **UFS-ESD2023/0001/23**

Please note the following:

1. **This ethical clearance is valid for two years from the issuance of this letter.**
2. **If the research takes longer than two years to complete, please submit a Continuation Report to the Ethics Committee before ethical clearance expires.**
3. **If any changes are made during the research process (including a change in investigators), please inform the Ethics Committee by submitting an Amendment.**
4. **When the research is concluded, please submit a Final Report to the Ethics Committee.**

Approved

Thank you for your application and we wish you well in all of your research endeavours.

Yours Sincerely

Prof. RR (Robert) Bragg
Chairperson: Environment & Biosafety Research Ethics Committee
University of the Free State

Directorate: Research Development
T: +27 (0)51 401 9398 | +27 (0)51 401 2075 | E: smitham@ufs.ac.za
Johannes Brill Building, Room 106D, First Floor
205 Nelson Mandela Drive | Park West, Bloemfontein 9301 | South Africa
P.O. Box 339 | Bloemfontein 9300 | South Africa | www.ufs.ac.za

Appendix B: Language editor letter

UNIVERSITY OF THE FREE STATE
UNIVERSITEIT VAN DIE VRYSTAAT
YUNIVESITHI YA FREISTATA
UFS UV

Centre for Teaching and Learning

31 July 2024

To whom it may concern,

I, Gawain Norval, hereby declare that I have proofread the master's dissertation entitled *ESTABLISHING A CISPLATIN-RESISTANT TRIPLE NEGATIVE BREAST CANCER SPHEROID MODEL*, by Ongeziwe Ngalonkulu

I am employed at the Unit for Academic Language and Literacy Development (ALLD), as a Facilitator of Academic Literacy within the ALLD at the University of the Free State (UFS). Due to my experience and expertise teaching Academic Literacy, I am intimately familiar with the structure and requirements of this dissertation and, therefore, qualified to edit, proofread, and verify the style and referencing for this document.

Please feel free to contact me should you require further information regarding the proofreading of this document, either telephonically, at 083 681 1546, or per email, at NorvalGT@ufs.ac.za.

Yours faithfully,

_____
Mr Gawain Norval
Unit for Academic Language and Literacy Development (ALLD)
Literacy Assistant: Unit for Academic Literacy

Unit for Academic Language and Literacy Development (ALLD)

205 Nelson Mandela Rylaan/Drive, Parkwes/Park West, Bloemfontein 9301, Suid-Afrika/South Africa
Posbus/P.O. Box 339, Bloemfontein 9300, Suid-Afrika/South Africa, Tel: +27(0)51 401 9111, www.ufs.ac.za